Neuron
Article

Presynaptic Partners of Dorsal Raphe Serotonergic and GABAergic Neurons

Brandon Weissbourd,[1] Jing Ren,[1] Katherine E. DeLoach,[1] Casey J. Guenthner,[1,2] Kazunari Miyamichi,[1,3,*] and Liqun Luo[1,2,*]
[1]Department of Biology and Howard Hughes Medical Institute
[2]Neurosciences Graduate Program
Stanford University, Stanford, CA 94305, USA
[3]Present Address: Department of Applied Biological Chemistry and JST ERATO Touhara Chemosensory Signal Project, Graduate School of Agricultural and Life Sciences, The University of Tokyo, Tokyo 113-8657, Japan
*Correspondence: amiyami@mail.ecc.u-tokyo.ac.jp (K.M.), lluo@stanford.edu (L.L.)
http://dx.doi.org/10.1016/j.neuron.2014.06.024

SUMMARY

The serotonin system powerfully modulates physiology and behavior in health and disease, yet the circuit mechanisms underlying serotonin neuron activity are poorly understood. The major source of forebrain serotonergic innervation is from the dorsal raphe nucleus (DR), which contains both serotonin and GABA neurons. Using viral tracing combined with electrophysiology, we found that GABA and serotonin neurons in the DR receive excitatory, inhibitory, and peptidergic inputs from the same specific brain regions. Embedded in this overall similarity are important differences. Serotonin neurons are more likely to receive synaptic inputs from anterior neocortex while GABA neurons receive disproportionally higher input from the central amygdala. Local input mapping revealed extensive serotonin-serotonin as well as GABA-serotonin connectivity with a distinct spatial organization. Covariance analysis suggests heterogeneity of both serotonin and GABA neurons with respect to the inputs they receive. These analyses provide a foundation for further functional dissection of the serotonin system.

INTRODUCTION

Understanding modulatory neurotransmitter and neuropeptide signaling will be indispensable for understanding information flow through neural circuits (Bargmann and Marder, 2013). There is a particularly urgent need for advances in this field, as the most widely prescribed drugs for neurological disorders target whole-brain modulatory signaling, yet often suffer from low efficacy and significant side effects (Nestler et al., 2009). The shortcomings of current brain-wide treatments suggest that it is essential to understand how these systems operate in the context of their specific connectivity—both in the inputs received by modulatory neurons, which direct the spatiotemporal patterns of their transmitter release, and in the interpretation of their output by the circuits being modulated. The need for such understanding is perhaps best exemplified by the monoamine modulatory transmitter serotonin, famous as the target system of the most widely prescribed class of antidepressants (Walker, 2013). Serotonin (5-hydroxytryptamine) is an ancient molecule that is instrumental in circuit function and behavior in diverse organisms, from *Aplysia* and *C. elegans* to mammals (e.g., Brunelli et al., 1976; Liu et al., 2011; Sawin et al., 2000). It has been implicated in various functions and dysfunctions of the mammalian brain: from feeding, aggression, sexual behaviors, and pain modulation to autism, schizophrenia, depression, and anxiety (reviewed in Müller and Jacobs, 2010).

The serotonin system exerts its widespread effects from a group of relatively small brainstem nuclei. Serotonin-producing neurons in these regions send ascending projections to the entire brain as well as descending projections to the spinal cord (Dahlström and Fuxe, 1964; reviewed in Hornung, 2010). These projections form classical synaptic connections as well as varicosities with no associated postsynaptic structure (Descarries et al., 2010). Upon release, serotonin acts primarily on G protein coupled receptors (and a single ionotropic receptor) encoded by more than a dozen distinct genes, and many more isoforms, that are differentially expressed in the brain (Bockaert et al., 2010).

The dorsal raphe (DR) is the largest serotonergic nucleus, containing more than half of the estimated 20,000 total serotonin-producing neurons in the rat (Descarries et al., 1982). It has been an area of intensive study due to its innervation of the forebrain and direct links to behavior, particularly related to stress, mood, and anxiety (Hale et al., 2012; Maier and Watkins, 2005). However, a number of other cell types are also present both within the DR and in closely apposed nuclei, including large and overlapping populations of GABAergic, glutamatergic, and dopaminergic neurons, many of which also produce various neuropeptides. In addition to heterogeneity with respect to transmitter synthesis, there is also considerable heterogeneity within serotonergic neurons (and these other cell types) with respect to connectivity, physiological properties, and receptor expression (e.g., Calizo et al., 2011; Kirby et al., 2003; Urbain et al., 2006; reviewed in Gaspar et al., 2003; Hale and Lowry, 2011).

To understand the circuits that control serotonergic modulation of animal behavior and physiology, it is essential to determine the direct synaptic inputs that control the activity of

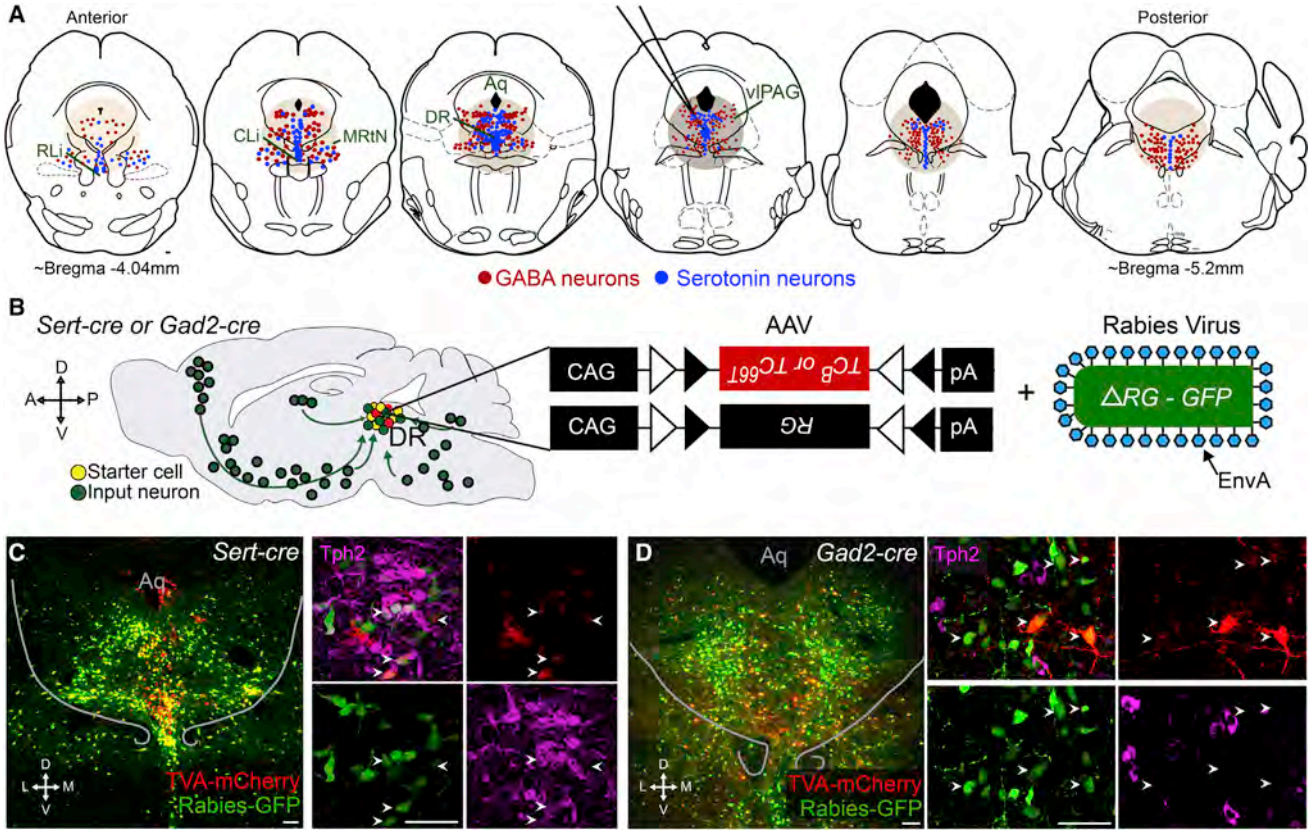

Figure 1. DR Serotonin and GABA Neurons as Starter Cells for Rabies-Based Transsynaptic Tracing

(A) Schematic representation of serotonin (blue) and GABA (red) neurons on coronal sections through the DR and surrounding regions, including the central and rostral linear nucleus raphe (CLi and RLi, respecitively), midbrain reticular nucleus (MRtN), and ventrolateral PAG (vlPAG). The approximate location targeted for viral injections and spread of infection is indicated with tan circles. Only serotonin and GABA neurons within these regions are drawn. Aqueduct (Aq).

(B) Schematic of rabies-based transsynaptic tracing. *Sert-cre* or *Gad2-cre* mice were transduced with two AAVs in the DR followed by EnvA-pseudotyped, glycoprotein (RG)-deleted, and GFP-expressing rabies virus. Serotonin or GABA starter cells are labeled in yellow, and presynaptic partners throughout the brain are labeled in green, as shown on a schematic sagittal section of the mouse brain. TC^{B}, wild-type TVA-mCherry fusion used in Figures 2–5; TC^{66T}, TVA-mCherry with a point mutation (66T) in the TVA receptor used in Figure 7; CAG, a ubiquitous promoter; triangles: loxP and Lox2272 sites that cause the transgene expression to be Cre dependent (FLEx).

(C) Left, 60 μm coronal section through the DR of a *Sert-cre* tracing brain showing the location of starter cells (yellow). Right, z projected confocal stacks of a different *Sert-cre* tracing brain in approximately the same position, triple labeled in green for GFP from rabies virus, in red for mCherry from TC^{B}, and in magenta with anti-Tph2 staining. All starter cells are Tph2 positive (arrowheads).

(D) Same as in (C), except from *Gad2-cre* tracing. Right panels show that none of the starter cells (arrowheads) are Tph2 positive.

Scale, 100 μm. In this and all other figures, abbreviations are as follows: A, anterior; P, posterior; D, dorsal; V, ventral; M, medial; L, lateral. Anatomical schematics and coordinates here and throughout are modified from Paxinos and Franklin (2001). Figure S1 describes further characterization of starter cell populations and the rabies tracing technique.

serotonin neurons. Previous studies using anterograde and retrograde tracers have identified numerous brain areas that send projections to the DR (reviewed in Hornung, 2010; Jacobs and Azmitia, 1992). While providing a valuable outline of possible inputs to DR cell types, most of these studies are limited by the inability to distinguish axons that pass by the DR from those that synapse onto DR neurons and, for the latter, the types of neurons onto which they synapse. The development of monosynaptic retrograde transsynaptic tracing based on modified rabies virus (Wickersham et al., 2007) has provided a means to systematically map the inputs to genetically defined populations of neurons in specific areas of the brain. Here we applied recently improved strategies for mapping both long-distance and local synaptic inputs (Miyamichi et al., 2013) to identify and compare neurons that send direct input to serotonin- and GABA-producing neurons in the DR.

RESULTS

Figure 1A shows the schematic organization of serotonin (blue) and GABA (red) neurons in the vicinity of the DR in a series of coronal sections. This schematic was based on immunostaining against tryptophan hydroxylase 2 (Tph2) to label serotonin-producing neurons (hereafter called serotonin neurons) and in situ hybridization (ISH) for *Gad1* and *Gad2*, encoding glutamate decarboxylases 1 and 2, to label GABA-producing neurons

(GABA neurons, hereafter) (Figures S1A, available online, and 7A). These clusters of serotonin neurons are distributed in continuous populations across multiple anatomical regions. However, they are mostly concentrated in the DR near the midline ventral to the aqueduct and in "wings" that extend into the ventrolateral periaqueductal gray (vlPAG). GABA neurons mostly flank these clusters of serotonin neurons, though at a finer scale, serotonin and GABA neurons are intermingled, including a small number of cells coexpressing *Gad1/2* and Tph2 (Figure S1A), consistent with previous reports (Belin et al., 1983; Shikanai et al., 2012). We chose a tracing protocol that would allow us to map with high efficiency inputs to the DR nucleus and these surrounding structures as a whole, despite losing subregion resolution. We will use "DR" to refer to these groups shown in Figure 1A for the remainder of this study.

Strategies for Tracing Inputs to DR Serotonin and GABA Neurons

Rabies-based, retrograde, transsynaptic tracing (Wickersham et al., 2007) relies on two modifications to the rabies virus that allow for (1) cell-type-specific initial infection with rabies and (2) monosynaptic spread from these cells. The first aim is achieved by using EnvA-pseudotyped rabies virus in combination with targeted expression of the cognate receptor (TVA) in specific cell types. The second aim is achieved using rabies glycoprotein (RG)-deleted rabies virus, allowing for rabies spread only when RG is provided in *trans*. To generate targeted rabies tracing, we used two Cre-dependent AAVs—expressing either TVA receptor-mCherry fusion or RG—in combination with mice that express Cre in specific cell types (Miyamichi et al., 2013; Watabe-Uchida et al., 2012). Starter cells are both mCherry+ (from the TVA-mCherry fusion) and GFP+ (from rabies virus), whereas their presynaptic partners are only GFP+.

We utilized two complementary strategies that differed in the TVA receptor used (Miyamichi et al., 2013). The first strategy utilizes an optimized construct expressing the wild-type TVA receptor-mCherry (TC^B), which allows for high-efficiency, long-range tracing, but exhibits considerable local background. The second strategy utilizes a mutant TVA receptor-mCherry (TC^{66T}), which lowers overall transsynaptic tracing efficiency compared to TC^B, but reduces background to ~0 (Miyamichi et al., 2013) (Figure S1). We used TC^B for whole-brain input mapping, excluding regions near the DR, and TC^{66T} for local input mapping.

To restrict starter cells to serotonin or GABA neurons, we used *Sert-cre* (Gong et al., 2007) and *Gad2-cre* (Taniguchi et al., 2011) mice, respectively. Figures 1C and 1D show examples of starter cells from *Sert-cre* (C) and *Gad2-cre* (D) experimental mice. Anti-Tph2 staining indicated that nearly all starter cells from *Sert-cre* tracing were Tph2 positive, while starter cells from *Gad2-cre* tracing were predominantly Tph2 negative (Figures 1C and 1D, inset; Figure S1B). Consistent with our previous result (Figure S1A), ~5% of starter cells from *Gad2-cre* tracing were Tph2 positive (Figure S1B; see Figure S1 and Supplemental Experimental Procedures for discussion of the rabies tracing technique as applied to the DR). Together, these experiments validated our strategy of tracing input to largely distinct populations of DR serotonin and GABA neurons.

Long-Range Inputs to DR Serotonin and GABA Neurons

To determine the presynaptic partners of DR serotonin and GABA neurons, we analyzed serial coronal (Figures 2A and 2B) and horizontal (Figure 2C) sections following TC^B-based transsynaptic tracing. Sections from representative *Sert-cre* (Figures $2A_1$–$2A_5$ and $2C_1$–$2C_6$) and *Gad2-cre* (Figures $2B_1$–$2B_5$) brains revealed rabies-GFP+ presynaptic input neurons located only in specific brain nuclei in a bilaterally symmetrical manner. Figure S2 provides horizontal and sagittal projections from 3D-reconstructed coronal sections. Overall, DR serotonin and GABA neurons receive input from the same brain regions. Images from a *Sert-cre* and a *Gad2-cre* tracing experiment are available at http://web.stanford.edu/group/luolab/DR.shtml.

The densest long-range labeling, from anterior to posterior, was observed in anterior neocortex (Figures $2A_1$ and 2C); extended amygdala (EAM), including the bed nucleus of the stria terminalis (BNST) (Figures $2A_2$ and $2C_3$–$2C_6$); lateral habenula (LHb), central amygdala (CeA), and subregions of the hypothalamus (Figures $2A_3$ and 2C); substantia nigra and ventral tegmental area (Figures $2A_4$, $2C_4$, and $2C_5$); as well as deep cerebellar nuclei (DCN) and the medulla (Figures $2A_5$, $2C_2$, and $2C_4$–$2C_6$). Despite very dense labeling of these input sites, large regions of the brain were either blank or sporadically labeled. These regions include the olfactory bulb, anterior olfactory nucleus, dorsal striatum, hippocampus, and the majority of the thalamus. While the central and EAM were densely labeled, there was little labeling in the medial, basolateral, and cortical amygdala.

To determine the overall distribution of the long-range, presynaptic partners of DR serotonin and GABA neurons, we divided each brain into 33 regions of interest and counted the number of cells in each (see Experimental Procedures). These regions accounted for nearly all long-range inputs, omitting the densely labeled midbrain and pons, which were excluded due to possible background from TC^B-based tracing. Data from four *Sert-cre* brains and four *Gad2-cre* brains representing those with high-efficiency tracing and starter cells most restricted to the DR were used in the quantitative analysis described below (Figures S3 and S4).

On average, tracing from serotonin neurons yielded higher numbers of long-range GFP+ cells (3,919, 27,582, 35,778, and 50,862 cells per mouse) than tracing from GABA neurons (2,697, 6,291, 11,862, and 12,665 cells per mouse). This difference cannot be accounted for by differences in starter cell numbers (2,147 ± 556.9, *Sert-cre* and 3,402 ± 1,940, *Gad2-cre*; mean ±SEM). As each brain had a different total number of input cells, in order to directly compare between experiments, for each mouse we plotted these counts as the fraction of input neurons counted within a given region over the total number of input neurons (Figures 2, 3, and 5).

Grouping the 33 subregions that we quantified into eight large regions, and considering the serotonin and GABA tracing brains together, the hypothalamus contributed most of the long-range inputs to the DR, followed by the amygdala, medulla, cortex, thalamus, cerebellum, striatum, and hippocampus (Figure 2D). The hippocampus was excluded from further analysis due to lack of labeling. Even at this coarse resolution, DR serotonin neurons received a higher proportion of their inputs from the cortex (2-fold enrichment, Figure 2D).

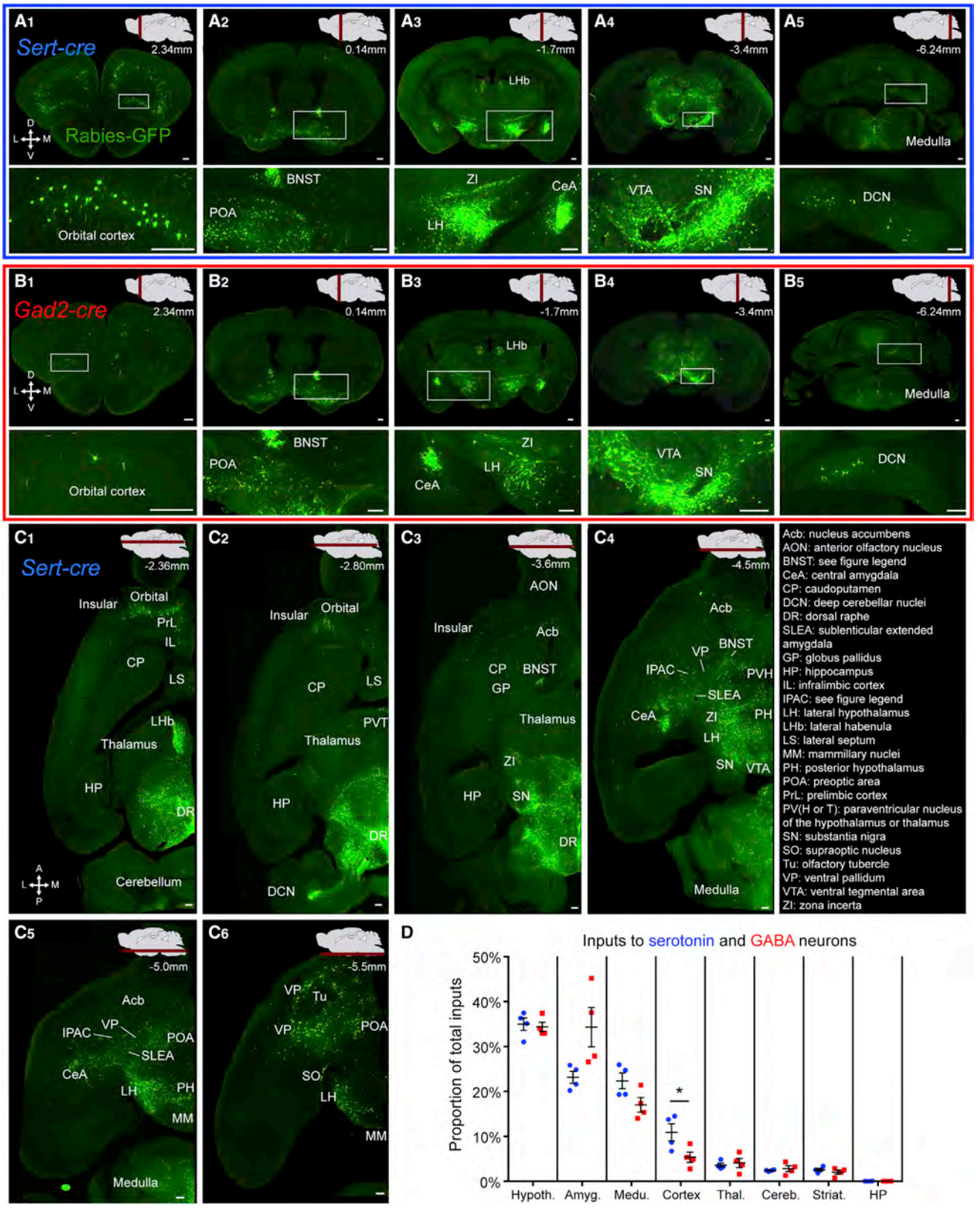

(legend on next page)

Serotonin and GABA Neurons Receive Specific Subcortical Input

To investigate input tracing in more detail, we first compared the distribution of inputs to DR serotonin and GABA neurons from subregions of interest in subcortical areas (Figure 3; Table S1). To test whether these subregions send excitatory or inhibitory inputs, we combined TC^B-based rabies tracing with ISH using *vGlut1/2* or *Gad1/2* probes, respectively.

Across subregions, the distribution of inputs from *Sert-cre* versus *Gad2-cre* tracing experiments was significantly different ($p < 0.0001$, two-way ANOVA), and projections from each of the large regions above (Figure 2D) were mostly from a specific subset of subregions. For example, thalamic inputs to both DR cell types were predominantly from the LHb, which accounted for 87% ± 2% of thalamic inputs (*Sert* and *Gad* pooled, Figure 3A_1). LHb and PVT inputs were predominantly *vGlut2* positive (Figure 3A_2), though we also observed sparse *Gad1/2*-positive projection neurons in the LHb (Figure 3A_3). From within the cerebellum, greater than 95% of inputs to both serotonin and GABA neurons came from the DCN (Figure 3B_1), which sent glutamatergic (Figure 3B_2) and not GABAergic (Figure 3B_3) projections.

The hypothalamus contributes similar proportions of inputs to both DR serotonin and GABA neurons, with 34% of hypothalamic inputs coming from the lateral hypothalamus (*Sert* and *Gad* pooled, Figure 3C_1). While no differences in hypothalamic input to serotonin and GABA neurons reach statistical significance, there are notable trends. These include the particularly large proportions of input to serotonin neurons from the lateral hypothalamus and to GABA neurons from the parasubthalamic nucleus (Figure 3C_1). The lateral hypothalamus contains both *vGlut*- and *Gad*-positive inputs to both serotonin and GABA neurons (estimated 2-fold more *Gad*-positive overall) with considerable variation between subregions of the LH (Figures 3C_2–3C_5).

We next subdivided the amygdala complex into four regions: the CeA, EAM (see Experimental Procedures for definition), BNST, and the remaining amygdalar nuclei combined. We found that three subdivisions account for nearly all amygdalar projections to the DR: the EAM, CeA, and BNST (Figure 3D_1). While the EAM makes up a similar proportion of the total inputs to serotonin and GABA neurons, the CeA makes up a significantly larger proportion of inputs to GABA neurons (2.8-fold enrichment) and sends GABAergic projections (Figures 3D_2–3D_4). The BNST has a notable trend toward projecting to DR GABA neurons and sends GABAergic projections from the dorsal BNST (Figures 3D_1 and 3D_5–3D_7), though sparse *vGlut2*-positive inputs to the DR exist in other BNST subregions (Figure 3D_5).

In summary, inputs to serotonin and GABA neurons come from specific subcortical structures. Embedded in the overall similarity between *Sert-cre* and *Gad2-cre* tracing experiments are considerable differences in input distribution, including striking differences in the central amygdala.

DR Neurons Receive Inputs from Diverse Cell Types in the Central Amygdala and Paraventricular Hypothalamic Nucleus

Much like the DR, each anatomically defined subregion that we have focused on thus far contains a complex and heterogeneous group of neurons. We next combined TC^B-based transsynaptic tracing from *Sert-cre* or *Gad2-cre* mice with ISH to identify the cell types from within the biased CeA and unbiased PVH that send inputs to DR serotonin and GABA neurons.

The central amygdala is composed of many populations of cells, including subsets that produce neuropeptides. From the Allen Brain Atlas (Lein et al., 2007), we identified four neuropeptide-encoding genes *Tac1*, *Tac2*, *Preproenkephalin*, and *Crh* (encoding corticotropin-releasing hormone) that are expressed in subsets of CeA neurons; we also included PKC∂, a marker of a functional subset of CeA neurons (Haubensak et al., 2010). We found that *Tac2*-positive neurons account for ~40% of the CeA inputs to both serotonin and GABA neurons (Figures 4A_1–4A_4), whereas *Pkc∂*+ projections account for ~8% (*Sert-cre* and *Gad2-cre* experiments pooled; Figures 4B_1–4B_4). There were no significant differences in the proportion of CeA inputs from either cell type projecting to DR serotonin versus GABA neurons. We also observed many *Crh*-positive inputs from the CeA to both serotonin and GABA neurons in the DR (21% pooled average), as well as sparse inputs from *Preproenkephalin*- (to both serotonin and GABA neurons) and *Tac1*-expressing neurons (only serotonin neurons tested) (Figure S5).

Thus, inputs to serotonin and GABA neurons from the central amygdala are from a mixture of cell types, this mixture is of similar proportions, and a *Tac2*-expressing population accounts for a large fraction of central amygdala input to DR neurons. *Tac2* is a member of the Tacykinin family of propeptides that produces

Figure 2. Overview of Whole Brain Input to DR Serotonin and GABA Neurons

(A and B) Coronal sections of a *Sert-cre* (A) and a *Gad2-cre* (B) tracing brain showing the distribution of presynaptic partners. Approximate section planes are shown in the top right on a sagittal section of a schematic brain, with approximate distance (anterior-posterior) from the bregma. Images at the bottom are higher magnification views of the rectangular regions on the top images.

(C) Six horizontal sections of one hemisphere of a *Sert-cre* tracing brain showing the location of presynaptic partners. Approximate section planes and distances from bregma are shown in the top right on a schematic sagittal brain section.

(D) Inputs to DR serotonin or GABA neurons from eight brain regions, shown as the proportion of the total cells counted that are located in a region. Dots represent four individual *Sert-cre* (blue) and *Gad2-cre* (red) tracing experiments. Serotonin neurons receive a greater proportion of their input from the cortex. BNST, bed nucleus of the stria terminalis; IPAC, interstitial nucleus of the posterior limb of the anterior commissure; Hypoth, hypothalamus; Amyg, amygdala; Medu, medulla; Thal, thalamus; Cereb, cerebellum; Striat, striatum; HP, hippocampus.

Scale, 250 μm. Statistical analysis here, and in Figures 3 and 5, used two-way ANOVA on normalized cell counts with Bonferroni corrections (see Experimental Procedures). Hypothalamus values are underestimates, as not all subregions were counted (see Table S1). In this and subsequent figures, error bars indicate SEM. Significance notation: *$p < 0.05$; **$p < 0.01$; ***$p < 0.001$. Figure S2 shows horizontal and sagittal views of inputs to DR serotonin and GABA neurons from 3D-reconstructed coronal sections. Figures S3 and S4 show starter cell distributions for each of the eight experiments used.

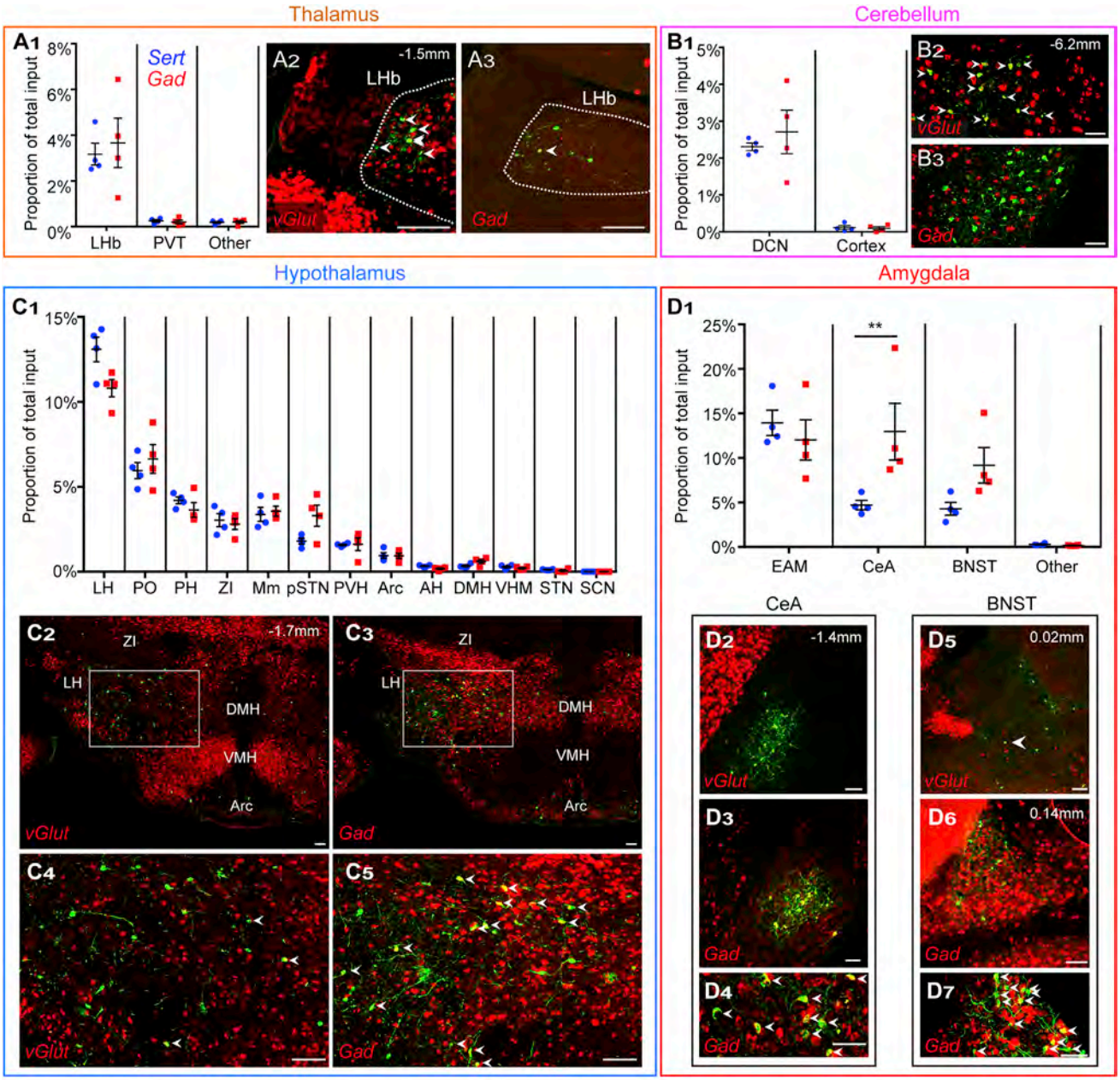

Abbreviations: LHb, lateral habenula; PVT, periventricular nucleus of the thalamus; DCN, deep cerebellar nuclei; LH: lateral hypothalamus; PO, preoptic areas; PH, posterior hypothalamic nucleus; ZI: zona incerta; Mm, mammillary nuclei; pSTN, parasubthalamic nucleus; PVH, paraventricular nucleus of the hypothalamus; Arc, arcuate nucleus; AH, anterior hypothalamic nucleus; DMH, dorsomedial hypothalamic nucleus; VMH, ventromedial hypothalamic nucleus; STN, subthalamic nucleus; SCN, suprachiasmatic nucleus; EAM, extended amygdala; CeA, central amygdala; BNST, bed nucleus of the stria terminalis.

Figure 3. Quantitative Analysis of Subcortical Input Distribution

Inputs to DR serotonin or GABA neurons from subregions of the groups shown in Figure 2D. As in Figure 2, dots represent four individual *Sert-cre* (blue) and *Gad2-cre* (red) tracing experiments and are shown as the proportion of the total cells counted in an experimental brain located in a given subregion. Accompanying photomicrographs show glutamatergic or GABAergic projections from subregions of interest. Green, rabies-GFP; red, ISH using a *vGlut1* and/or *vGlut2* probe or a *Gad1+2* probe mix. All arrowheads point to double-labeled cells. Values in the upper right indicate approximate distance from bregma for each set of images.

(A) (A_1) Proportion of total inputs from thalamic subregions. Inputs from the thalamus are almost entirely from the lateral habenula (LHb) and glutamatergic (A_2), though we observe sparse LHb GABAergic presynaptic neurons as well (A_3).

(B) (B_1) Proportion of total inputs from the cerebellum. Inputs from the cerebellum are almost entirely from the deep cerebellar nuclei (DCN) and are glutamatergic (B_2) and not GABAergic (B_3).

(legend continued on next page)

neurokinin B, which is involved in the regulation of sexual maturation and function in the hypothalamus (Lasaga and Debeljuk, 2011), but whose role in the CeA remains unknown. As we have shown that the CeA makes up a larger proportion of inputs to DR GABA neurons (Figure 3D_1), these cell types are likely to disproportionately affect DR GABA neuron function.

We next used the same strategy to identify subsets of PVH neurons that project to DR serotonin and GABA neurons. Cells in the PVH express *vGlut2* and rarely *Gad1/2*; consistent with this observation, we see many *vGlut2*-positive but no *Gad1/2*-positive inputs from the PVH to the DR (Figures 4E_1 and 4E_2). We next labeled oxytocin- or vasopressin (AVP)-producing neurons and observed that both serotonin and GABA neurons receive inputs from both cell types (Figures 4C and 4D) and that numerous oxytocin (Figure 4E_3) and AVP (Figure 4E_4) neurons in the PVH also express *vGlut2*.

AVP and oxytocin inputs were consistent across *Sert-cre* tracing experiments, with a trend toward preferential targeting of serotonin neurons by AVP (Figure 4C_4). However, there was high variability between *Gad2-cre* samples (Figure 4C_4), similar to the *Gad2-cre*-specific high variation in the PVH seen in the subregion mapping above (Figure 3C_1). This suggests that PVH populations may target specific subsets of DR GABA neurons, making tracing results more susceptible to differences in the starter cells sampled (see Figure 8; Discussion).

Anterior Cortical Neurons Send Biased Input to DR Serotonin Neurons Compared to GABA Neurons

The connectivity between the anterior cortex and the DR has attracted great interest as a circuit involved in modulating stress and depressive behaviors (Amat et al., 2005; Warden et al., 2012). Interestingly, our analysis of large brain structures suggests that the cortex as a whole preferentially targets serotonin neurons (Figure 2D). We therefore investigated cortical input patterns in more detail by first counting the number of labeled cells in seven subregions of the neocortex (Figures 5A and 5B).

We found that the insular cortex made up a larger proportion of inputs to DR serotonin neurons compared to DR GABA neurons (Figures 5B, 5D, and 5E). We also observed smaller but significant biases in the orbital and prelimbic/cingulate (PrL/Cg) cortices toward DR serotonin neurons (Figures 5B, 5D, and 5E). These input neurons from the cortex to the DR are glutamatergic (Figures 5F_1 and 5F_2). The anterior-posterior distributions of cortical inputs were similar for *Sert-cre* and *Gad2-cre* brains, with strong bias toward anterior cortical regions (Figures 5C–5E). Thus, the anterior cortex in general, and the insular cortex in particular, sends biased input to DR serotonin neurons compared to GABA neurons.

To test whether the biased input from anterior cortex to DR serotonin neurons over GABA neurons reflects biased functional connections, we employed channelrhodopsin-assisted circuit mapping (CRACM) (Petreanu et al., 2007) to examine connectivity rates. We first transduced anterior cortical neurons of *Sert-cre* or *Gad2-cre* mice with an AAV expressing ChR2-EYFP, aiming to fill a large proportion of anterior cortex. Four weeks later, we transduced the DR with an AAV expressing Cre-dependent mCherry to label either serotonin or GABA neurons. Two weeks later, acute coronal DR slices were used for whole-cell patch recording in response to photostimulation of cortical axon terminals (Figure 6A).

All animals with expression of ChR2 in the anterior cortex (n = 8 *Sert-cre* mice, n = 8 *Gad2-cre* mice) had bright EYFP+ axon fibers in DR slices (Figure 6B), indicating direct projections from anterior cortical neurons. In voltage-clamp mode, brief blue light illumination (5 ms) evoked immediate excitatory postsynaptic potentials (EPSCs) in a subset of mCherry+ serotonin and GABA neurons when cells were held at −65 mV (Figure 6C_1). These responses were eliminated by application of 6,7-dinitroquinoxaline-2,3-dione (DNQX; 10 μM), a selective antagonist of AMPA-type glutamate receptors (Figures 6C and 6D), indicating that anterior cortical axons release glutamate (n = 7). The short latency as well as pharmacological inhibition and reinstatement (Figure S6) indicate that these connections are monosynaptic.

Of a total of 43 serotonin neurons from four *Sert-cre* mice, 15 cells (35%) exhibited EPSCs in response to photostimulation. Of the 57 GABA neurons recorded from five *Gad2-cre* mice, only nine cells (16%) produced EPSCs in response to photostimulation (Figure 6E). Post hoc staining of neurobiotin-filled cells that received direct input from anterior cortex confirmed their cell type identity and their location within the DR (Figures 6B). These results demonstrate monosynaptic, glutamatergic inputs from anterior cortical neurons onto a subset of DR serotonin and GABA neurons, with a higher connectivity rate with serotonin neurons. This is consistent with our transsynaptic tracing results showing that serotonin neurons receive a greater fraction of their inputs from the anterior cortex (Figure 5B). Interestingly, DR GABA neurons that received direct anterior cortical input were preferentially concentrated in the ventral wing (Figure 6F).

Anterior Cortical Inputs to DR Serotonin and GABA Neurons Exhibit Different Postsynaptic Properties

In addition to anatomical connectivity, functional differences may be present in the synaptic properties of these connections. We therefore examined the postsynaptic properties of cortex-to-DR connections by characterizing the voltage dependence of photostimulation-induced EPSCs. Both cell types exhibited relatively large EPSCs at hyperpolarized holding potentials, while

(C) (C_1) Proportion of total inputs from subregions of the hypothalamus. The lateral hypothalamus (LH) makes up the majority of hypothalamic input, though many regions send considerable projections to the DR. The LH sends both glutamatergic and GABAergic projections ([C_2]–[C_5]).
(D) (D_1) Proportion of total inputs from subregions of the amygdala. The central amygdala (CeA) makes up a larger proportion of total input to DR GABA compared to serotonin neurons (Bonferroni correction against the 33 subregion comparisons). The central amygdala sends GABAergic and not glutamatergic input ([D_2]–[D_4]). The dorsal BNST sends GABAergic input ([D_6] and [D_7]), and we have seen sparse vGlut2+ projections from other subregions (D_5).
Scale, 100 μm. Abbreviations color code are as follows: subregions of the thalamus (orange), cerebellum (magenta), hypothalamus (blue), and amygdala (red). Table S1 contains cell counts for each subregion, including those not shown here, and qualitative information on subregions not counted.

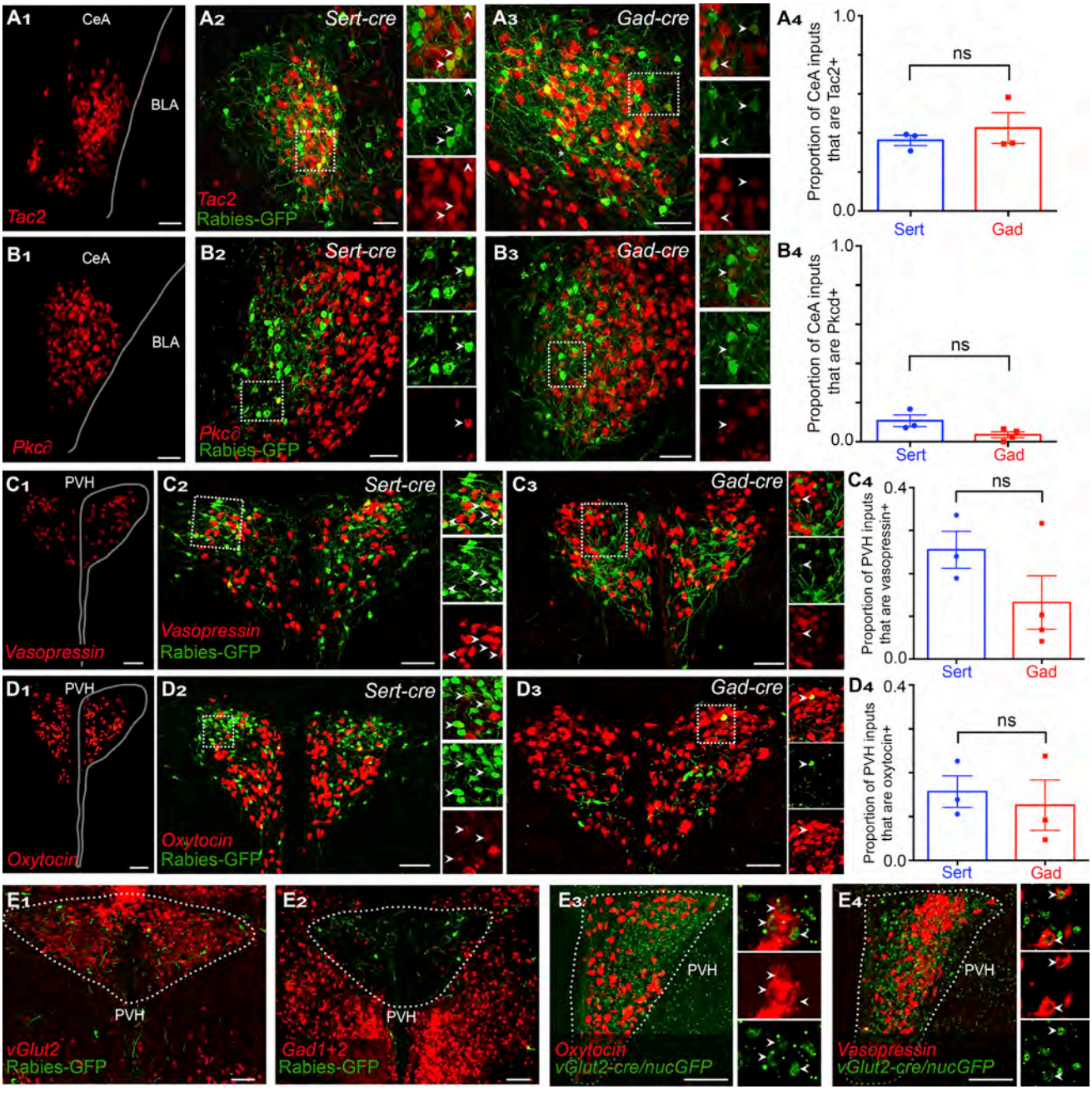

Figure 4. Characterizing DR Input Cell Types in the Central Amygdala and Paraventricular Hypothalamic Nucleus

(A and B) Central amygdala sections with *Tac2* (A) or *Pkcδ* (B) ISH (red), alone with anatomical boundaries ([A_1] and [B_1]) or in a *Sert-Cre* ([A_2] and [B_2]) or a *Gad2-Cre* ([A_3] and [B_3]) brain; quantification of GFP+ cells that are *Tac2*+ or *Pkcδ*+ is also shown ([A_4] and [B_4]). High magnification images to the right of each image correspond to boxes in the low magnification images to the left. BLA, basolateral amygdala.

(C and D) PVH sections with *vasopressin* (C) or *oxytocin* (D) ISH (red) alone with anatomical boundaries ([C_1] and [D_1]) or in a *Sert-cre* ([C_2] and [D_2]) or a *Gad2-Cre* ([C_3] and [D_3]) brain; quantification of GFP+ cells that express *vasopressin* (C_4) or *oxytocin* (D_4) is also shown.

(E) PVH projections to the DR are *vGlut2* positive (E_1) and not *Gad1/2* positive (E_2). Populations of both *oxytocin* (E_3) and *vasopressin* (E_4) neurons coexpress *vGlut2*.

Scale, 100 μm. All arrowheads (except in [E_3] and [E_4]) indicate double-labeled cells for GFP from rabies virus and ISH probes. Analysis by two-tailed, unpaired t tests followed by Bonferroni correction. Each data point represents one experimental animal. Figure S5 shows additional cell types that send input to DR serotonin and GABA neurons from the CeA.

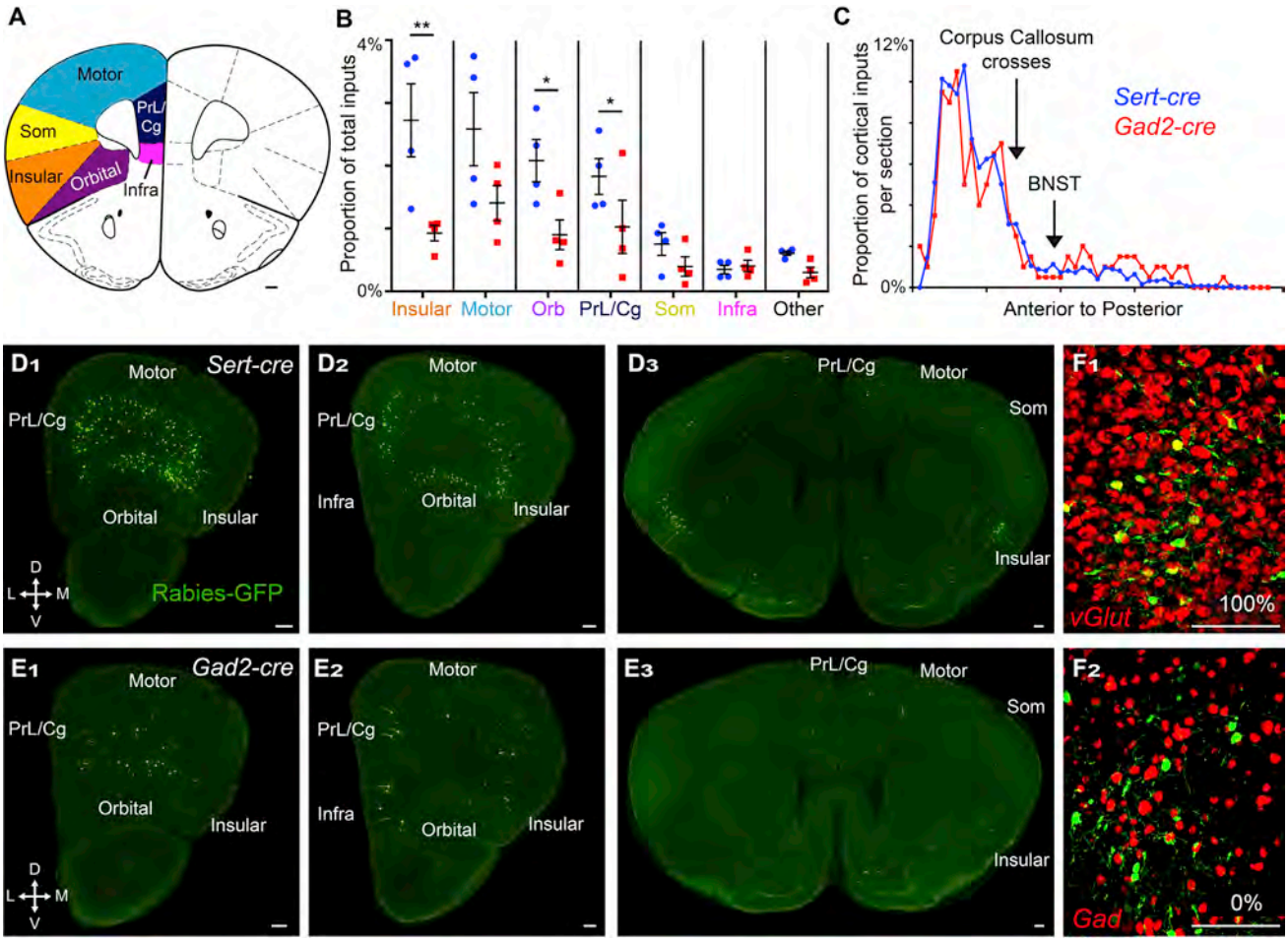

Figure 5. Quantitative Analysis of Cortical Input Distribution

(A) Schematic showing the location of cortical subregions quantified in (B) at one of the many coronal planes quantified.

(B) Inputs to DR serotonin (blue) or GABA (red) neurons from subregions of the anterior cortex. Serotonin neurons receive a higher proportion of their total input from insular, orbital (orb), and prelimbic/cingulate (PrL/Cg) cortices. "Other" includes all other neocortical regions.

(C) Neocortex input neurons per coronal section from anterior (left) to posterior in a representative *Sert-cre* (blue) and *Gad2-cre* (red) brain. The first crossing of the corpus callosum and the anterior border of the BNST indicated on graph.

(D and E) Coronal sections of a *Sert-cre* (D) and a *Gad2-cre* (E) brain with the locations of cortical subregions indicated.

(F) Cortical projections are all glutamatergic (F_1) and not GABAergic (F_2).

Scale, 200 μm. Som, somatosensory cortex; Infra, infralimbic cortex.

GABA neurons showed much smaller outward current at depolarized potential (Figures 6G and $6H_1$). Thus, in contrast to serotonin neurons whose *I–V* curve was generally linear, GABA neurons showed a rectified *I–V* curve (Figure 6I) with (green line) or without (red line) the NMDA receptor antagonist APV in the recording solution. This suggests that DR GABA neurons express GluA2-lacking AMPA receptors, which confer distinct synaptic properties compared to GluA2-containing AMPA receptors, including increased synaptic conductance and permeability to Ca^{2+} (Isaac et al., 2007). In addition, EPSCs in GABA neurons did not have a marked NMDA component (Figure $6H_1$). For five GABA neurons tested, APV (50 μM) had a relatively small effect on the EPSC when clamped at +60mV (Figures $6H_2$ and 6J, lower panel). In contrast, EPSCs in serotonin neurons exhibited an increased slow component when the holding potential went up from −40mV to +60mV (Figures 6G and 6J). In serotonin neurons that were treated with APV (n = 7 cells), the slow component was eliminated, indicating significant NMDA receptor contributions to postsynaptic currents of serotonin neurons (Figures 6G and 6J).

Serotonin Neurons Receive Diverse Local Input with a Specific Spatial Pattern

In order to control serotonin neuron activity, the complex, long-range inputs that we have described thus far interact with a largely uncharacterized local DR circuit containing diverse cell types (see Introduction). Interestingly, the specific location of cortical inputs to DR GABA neurons in the CRACM experiments (Figure 6) further implies that there are spatially distinct subsets of DR serotonin and GABA neurons. To gain insight into how

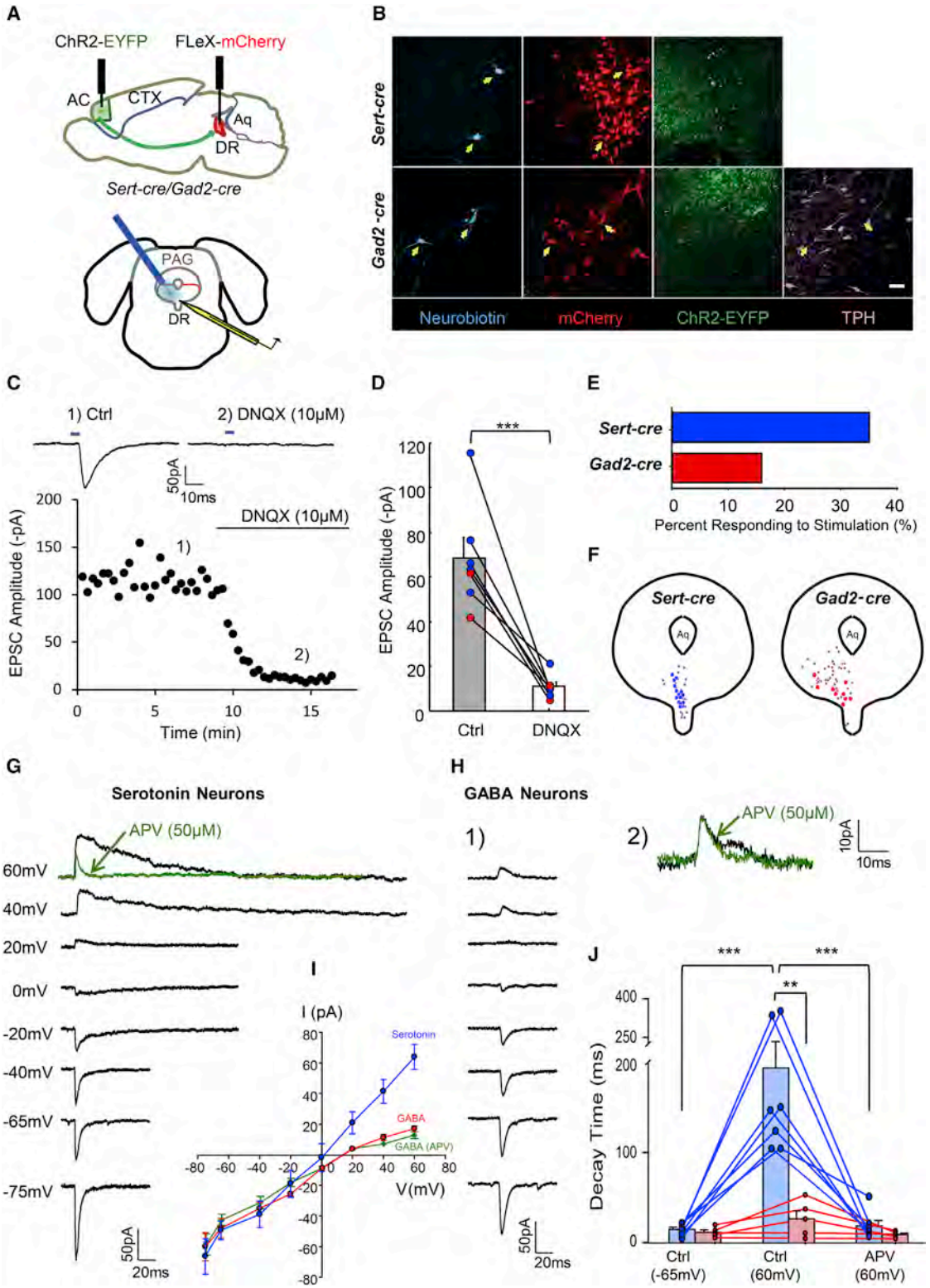

Figure 6. Connectivity and Synaptic Properties of Cortical Inputs to DR Serotonin and GABA Neurons

(A) Schematic drawing of virus injection and slice recording procedures. Top, sagittal view showing AAV_{DJ}-*CaMKII-ChR2(H134R)-EYFP* injection into anterior cortex (AC) of either *Sert-cre* (n = 6) or *Gad2-cre* (n = 5) mice. AAV_{DJ}-*EF1a-FLEx-mCherry* was injected into the DR to label serotonin or GABA neurons. Bottom,

(legend continued on next page)

serotonin neurons integrate long-range and local inputs, particularly in their interactions with DR GABA neurons, we next characterized local synaptic input to serotonin neurons utilizing the TC^{66T}-based tracing strategy with minimal local background (Figure S1E) (Miyamichi et al., 2013).

Figures 7A_1–7A_4 show coronal sections through the DR with rabies-GFP tracing from serotonin neurons combined with *Gad1/2* ISH. The DR and vlPAG contain large, distinct clusters of GABA neurons, and inputs to serotonin neurons are enriched in particular subregions. Interestingly, large regions of these neighboring DR GABAergic neurons were essentially unlabeled, particularly when compared to the very dense inputs from a nearby subregion of the midbrain reticular nucleus (MRtN) (e.g., Figure 7A_2). In contrast, we observed many Tph2-positive local inputs (Figures 7B_1 and 7B_2).

To quantify the spatial distribution of inputs, we subdivided the DR and nearby regions into three structures based on the pattern of *Gad1/2* ISH: dorsal wings (DWs), ventral wings (VWs), and the midbrain reticular nucleus (Figures 7C_1–7C_3) and grouped these subregions into four bins across the anterior-posterior axis (similar to Bang and Commons, 2012). We then quantified the number of local inputs to serotonin neurons that were coming from each of these subregions. Beginning with all local inputs regardless of their cell type, we found that the three subdivisions contributed similar input, as the DWs accounted for 35% ± 5% of the total input, the VWs for 27% ± 4%, and the MRtN for 38% ± 7%. When the spatial distribution of local inputs was analyzed using heatmaps to show relative enrichment of a subregion along the A-P axis, it was evident that specific subregions were responsible for the majority of local inputs (Figure 7E).

We next examined the distribution of cell-type-specific inputs to DR serotonin neurons. Surprisingly, local inputs were as likely to be from other serotonin neurons (41% ± 6%) as from neighboring GABA neurons overall (39% ± 0.7%, Figure 7D). This is likely an underestimate of serotonin-serotonin connectivity, as the subregions we used to analyze local input (Figure 7C) excluded serotonin neurons on the midline, where local serotonin inputs were densely intermingled with starter cells. The roughly 20% that is unaccounted for is composed of multiple cell types, including *vGlut1-3*+ input, notably from the *Gad*-negative, anterior PAG clusters in Figure 7A_1 (data not shown).

We next looked at the spatial distributions of *Gad1/2*- and Tph2-positive inputs across the subregions described above (Figures 7F and 7G). Local GABAergic input primarily came from the MRtN (Figure 7F_1), while serotonergic inputs were more evenly distributed across the MRtN, DWs, and VWs (Figure 7G_1). Further, GABAergic and serotonergic local inputs to DR serotonin neurons came from specific subregions along the A-P axis: serotonergic local inputs were enriched in the ventral and DWs in the central DR, while GABAergic local inputs were mostly from posterior DWs and the anterior midbrain reticular nucleus (Figures 7F_2 and 7G_2).

In summary, these results demonstrate the diversity of local input and the presence of a specific spatial organization—including the finding that an MRtN subregion sends dense inputs to DR serotonin neurons. These results also suggest, conditional to the caveats of rabies-based tracing, that many local GABA neurons may not play a major role in directly inhibiting DR serotonin neurons.

Covariance between Input Regions Suggests DR Circuit Heterogeneity

Our analysis of local inputs suggests that the DR is highly heterogeneous with spatially distinct populations. In our analysis of long-range tracing, we see considerable variability between animals, with particular input regions varying more than others. This variability may indicate that starter cells in each experiment sample from subpopulations of DR neurons that have different underlying connectivity. We therefore explored the variability between experiments in more detail. To increase the number of independent samples, and to validate our previous findings, we quantified the number of cells in the anterior cortex (anterior to the corpus callosum crossing), central amygdala, medulla, LHb, PVH, and BNST for a replication cohort of three *Sert-cre*

whole-cell recording from mCherry+ cells in coronal sections containing the DR coupled with the laser stimulation from an optical fiber placed immediately above the DR.

(B) Confocal z projections showing recorded DR serotonin (upper panels) and GABA (lower panels) neurons filled with neurobiotin during recording (cyan) together with mCherry (red) and axon terminals from ChR2-EYFP-expressing anterior cortical neurons (green). Arrows point to neurobiotin-labeled neurons within the area covered by ChR2-EYFP+ axonal terminals. All are mCherry+. *Gad2-cre* slices were stained with Tph2 antibody (pink); all neurobiotin-labeled neurons were negative for Tph2. Scale, 50 μm.

(C) EPSCs evoked by photostimulation (blue bar, 5 ms) are mediated by AMPA receptors. Stimulation-induced EPSCs (C_1) were abolished by application of DNQX (C_2), an AMPA receptor antagonist. Top traces are the average of six trials from the same serotonin neuron, with 20 s intertrial intervals. Bottom graph shows the change in EPSC amplitude over time. Each dot represents an EPSC generated by optical stimulation at fixed 20 s intervals.

(D) Summary data showing that the amplitudes of light-evoked EPSCs are almost completely abolished by the application of DNQX. Blue dots, serotonin neurons. Red dots, GABA neurons. Paired t test, n = 7 cells.

(E) Connectivity rate of anterior cortical input to DR serotonin (blue) and GABA neurons (red).

(F) Summary diagram showing the locations of recorded DR serotonin (blue, left) and GABA neurons (red, right). Purple, nonresponding cells. Aq, aqueduct.

(G) EPSCs of a DR serotonin neuron at different membrane potentials. APV application abolished the slow (NMDA receptor) component at +60mV (inset, green trace). Each trace is an average of six repeats.

(H) (H_1) EPSCs of a DR GABA neuron at different membrane potentials. (H_2) APV application had minimal effect on the EPSC at +60mV (inset, green trace). Each trace is an average of six repeats.

(I) *I/V* curves of serotonin (blue, n = 7) and GABA neurons with (green, n = 5) or without (red, n = 5) APV in the recording solution.

(J) Decay time of photostimulation-evoked EPSCs. For serotonin neurons (blue), decay time of EPSCs significantly increased at +60mV compared to −65mV and was dramatically reduced by APV application. Paired t test, n = 7 cells. For GABA neurons (red), little difference was seen between EPSCs recorded at −65mV, +60mV, or with APV application.

Figure S6 provides evidence that connections between anterior cortical axons and DR serotonin and GABA neurons are monosynaptic.

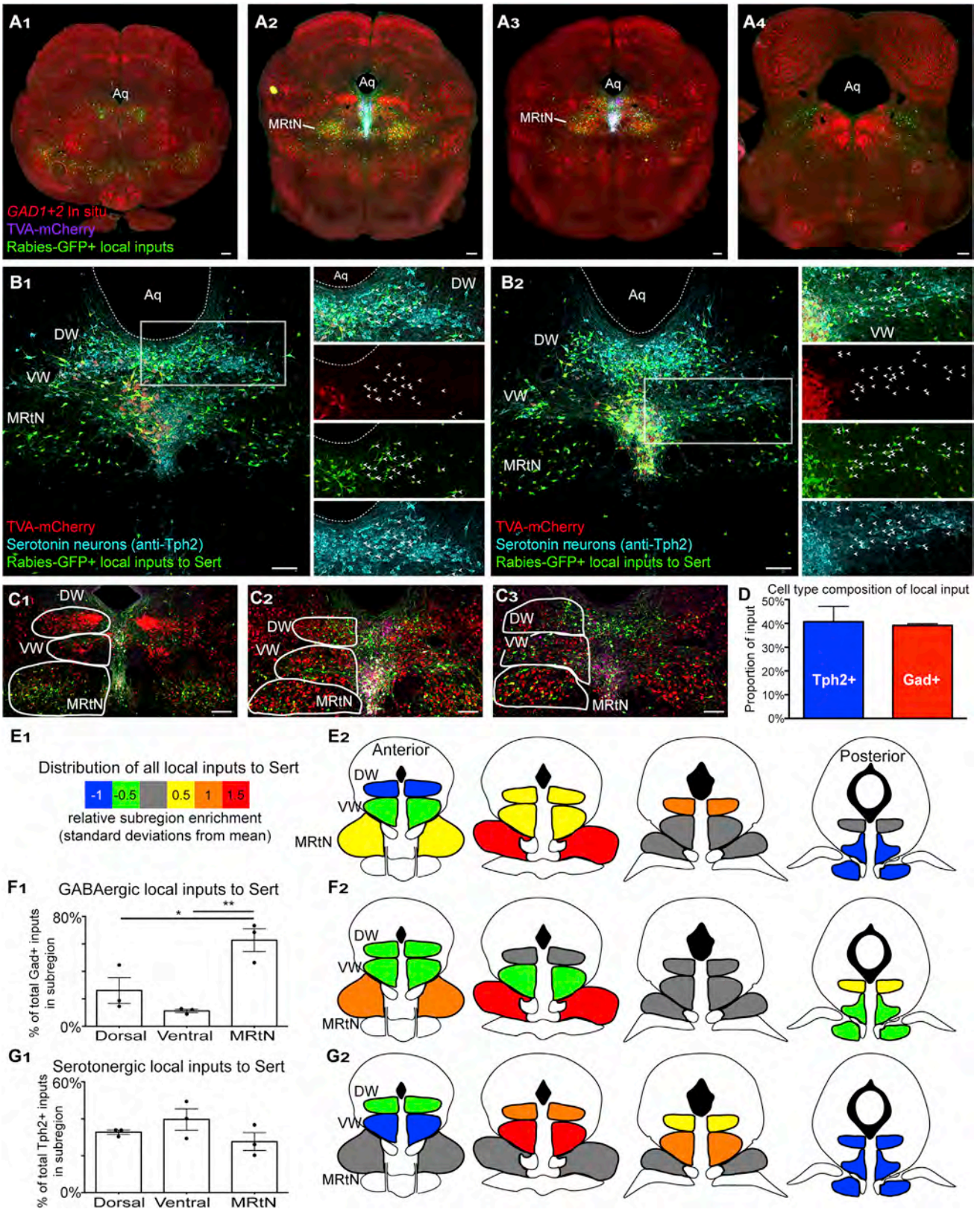

(legend on next page)

and four *Gad2-cre* tracing experiments. These new experiments support our previous findings, with the cortex and medulla making up a larger proportion of inputs to serotonin neurons and the CeA and BNST making up a larger proportion of inputs to GABA neurons (Figure S7).

When combining these replicate experiments with our eight previously analyzed brains, we observed that more sparsely labeled brains tended to be more variable, while densely labeled brains often trended toward the mean. This suggests that our tracing results may represent a sample drawn from subsets of DR neurons with differential connectivity, with high-efficiency brains more widely sampling from, and effectively averaging, these subsets. We therefore asked whether inputs from subregions were covarying, which might indicate that subpopulations in the DR receive long-range inputs from distinct combinations of brain regions and provide candidate pairs of regions that innervate the same subsets of cells.

Using the seven *Sert-cre* and the eight *Gad2-cre* experiments included above, we performed pairwise correlations followed by hierarchical clustering analysis between the six regions quantified. Interestingly, we observed considerable clustering in both *Sert-cre* and *Gad2-cre* cohorts (Figures 8A and 8B). For *Sert-cre* tracing, the LHb, PVH, and cortex formed a cluster separate from the medulla, CeA, and BNST. We observed a particularly strong negative correlation between the cortex and medulla (Figures 8A and 8C). Generally, clustering and correlations were more striking in *Gad2-cre* tracing experiments, with the CeA and BNST forming a particularly strong cluster distinct from the cortex, LHb, and medulla (Figure 8B). The medulla was negatively correlated with the CeA (Figure 8D) and BNST ($r = -0.84$), while the CeA was positively correlated with the BNST (Figure 8E). Additionally, the CeA and BNST were both negatively correlated with the cortex ($r = -0.72$ and -0.82, respectively).

This analysis suggests that subsets of DR serotonin and GABA neurons receive inputs from different combinations of regions. For example, serotonin neurons receiving cortical input may be largely distinct from those innervated by the medulla, and GABA neurons receiving CeA inputs may be the same as those receiving BNST input, yet distinct from those receiving cortical and medullary input. This could occur at the level of individual cells, small clusters, or large spatial regions, as our sampling of the DR is concentrated around a spatially defined injection site. Interestingly, *Gad2-cre* tracing experiments appeared more clustered, suggesting that DR GABA neurons are composed of distinct subsets more easily distinguishable with this technique.

DISCUSSION

DR serotonin and GABA neurons receive direct excitatory, inhibitory, and peptidergic input from diverse yet specific regions (Figure 8F). Glutamatergic neurons in the anterior cortex preferentially synapse onto DR serotonin neurons, whereas DR GABA neurons receive a higher proportion of their inputs from the GABAergic central amygdala. CRACM confirmed biased input of cortical projections to serotonin neurons and identified different postsynaptic properties of DR cell types. Analysis of local connectivity within the DR demonstrated that a large proportion of inputs to serotonin neurons are from other serotonin-producing cells and that local input comes from distinct spatial locations (Figure 8G). Analysis of long-range inputs also provides evidence for DR subcircuits and predicts which brain regions may preferentially coinnervate DR subpopulations. Below we discuss the limitations, advances, and implications of our study.

Caveats and Limitations

It is important to note that the precise mechanisms and possible caveats of rabies-based tracing are not entirely known, particularly as they apply to previously untested cell types and connections. It has been established in many systems that rabies virus spreads effectively across known synaptic connections (Haubensak et al., 2010; Miyamichi et al., 2011, 2013; Stepien et al., 2010; Takatoh et al., 2013; Ugolini, 1995; Watabe-Uchida et al., 2012; Wickersham et al., 2007) and does not infect axons in passage (e.g., Miyamichi et al., 2011). However, it is unknown whether there are biases in which synapses are crossed, and it is difficult to prove complete synaptic specificity in complex CNS circuits in vivo; for example, whether rabies virus will cross an axo-axonal synapse that is onto the presynaptic terminal of an input to a starter cell. Lastly, it is not known whether the

Figure 7. Distribution of Local Inputs to DR Serotonin Neurons

(A) Coronal sections (anterior to posterior) from a *Sert-cre* brain showing rabies-GFP+ local inputs (green) to serotonin neurons (TVA-mCherry, magenta) with *Gad1+2* ISH (red). Aq, aqueduct; MRtN, midbrain reticular nucleus.

(B_1 and B_2) Serotonergic local inputs to DR serotonin neurons from the dorsal (B_1) and ventral (B_2) wings. Right, staining in separate channels for regions indicated with white boxes. Arrowheads indicate Tph2+ local input neurons.

(C) Coronal sections with outlines indicating regions for quantification. DW, dorsal wing; VW, ventral wing.

(D) Proportion of local inputs to DR serotonin neurons coming from other serotonin neurons (blue) or GABA neurons (red); n = 3 tracing experiments.

(E) Spatial distribution of local input to DR serotonin neurons across DR subregions, regardless of their cell type. For each subregion, the proportion of total local input neurons was calculated and a heatmap was generated to indicate enrichment (red = most enriched; blue = least) using SD from the mean. Analysis based on n = 5 tracing experiments.

(F) The proportion of GABAergic local inputs to serotonin neurons located in each of the three subregions (F_1) and their spatial distribution (F_2). GABAergic inputs are largely from the MRtN compared to the dorsal (2.4-fold) and ventral (5.6-fold) wings (F_1). Inputs are mostly from anterior MRtN and posterior DWs (F_2). Spatial distribution shown as a heatmap, as in (E_2). Analysis of n = 3 tracing experiments by one-way ANOVA with Bonferonni correction.

(G) The proportion of serotonergic (Tph2-positive) local inputs to serotonin neurons located in each of the three subregions (G_1) and their spatial distribution (G_2). While serotonergic local input neurons are evenly distributed across the three subregions, their detailed spatial distribution shows dense inputs from the dorsal and ventral wings in the central DR. Analysis of n = 3 tracing experiments, as above.

Scale: 200 μm.

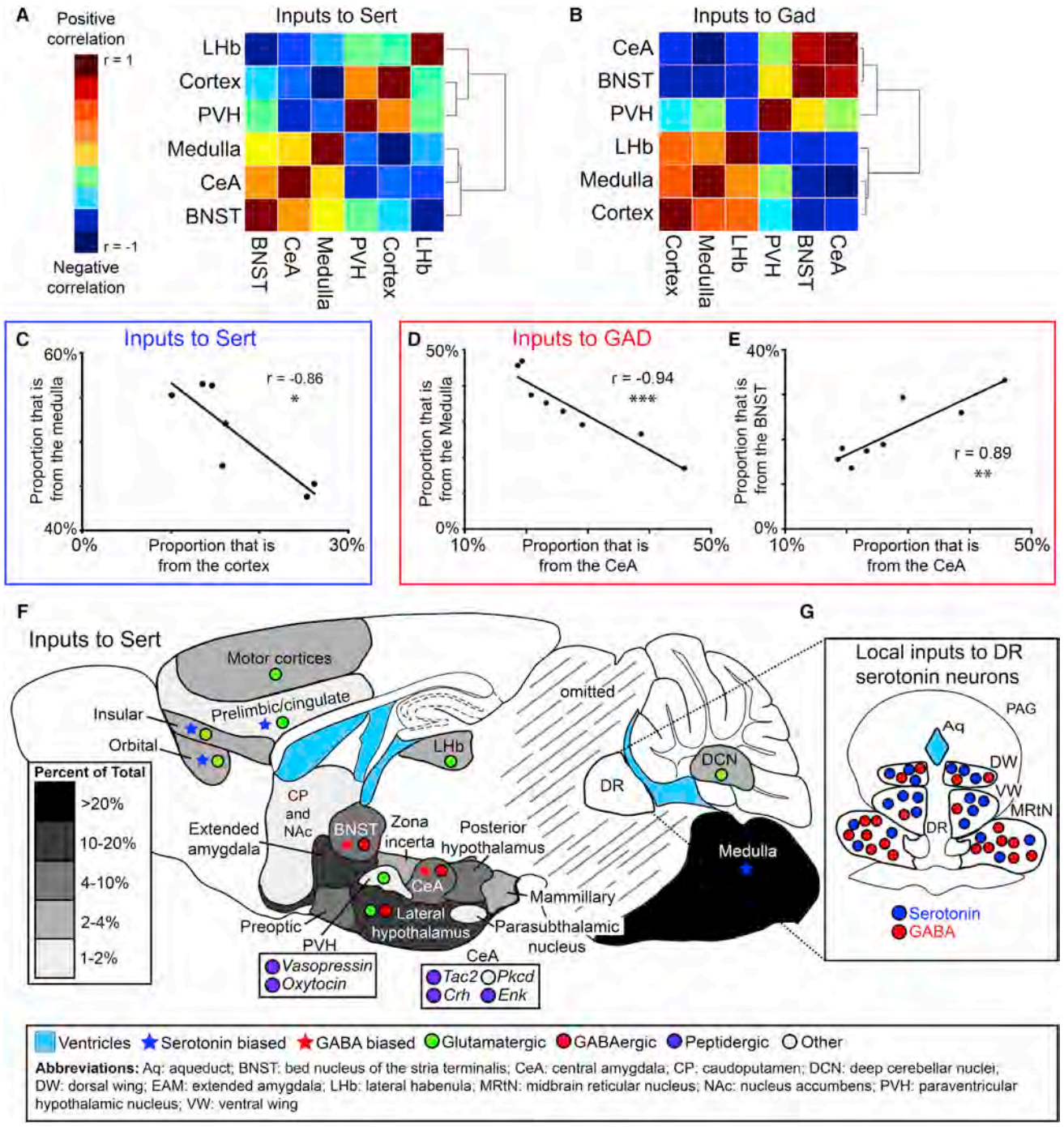

Figure 8. Covariance between Input Regions and Summary of Findings

(A and B) Pairwise correlations and cluster analysis of six regions counted in seven *Sert-cre* (A) and eight *Gad2-cre* (B) experiments. Heatmaps represent high correlation (red) or anticorrelation (blue) between regions. Cortex includes all neocortical regions anterior to the corpus callosum crossing.

(C–E) Example graphs showing a strong negative correlation between cortical and medullary inputs in *Sert-cre* tracing experiments (C), a strong negative correlation between central amygdalar and medullary inputs (D), and a strong positive correlation between inputs from the central amygdala and BNST (E) in *Gad2-cre* tracing experiments. Each dot is a separate tracing experiment. Values shown are Pearson correlation coefficients with uncorrected p values from a two-tailed test.

(F) Summary of inputs to the DR on a schematic sagittal section showing regions that make up greater than 1% of total inputs. Percentage of total input is coded by gray scales (inset). Stars indicate biased input to DR serotonin (blue) or GABA (red) neurons. The primary neurotransmitters expressed by input regions are shown as small circles as indicated in the inset.

(G) Schematic of local inputs to DR serotonin neurons. Blue, serotonergic inputs; red, GABAergic inputs. The number of circles in each region reflects the quantitative distribution of local inputs of each cell type.

differences in tracing efficiency observed between serotonergic and GABAergic neurons reflect real, underlying connectivity rates or are a result of the tracing technique and how this might affect input distribution.

A second limitation is that some DR neurons express both Tph2 and Gad2, so that serotonin and GABA input tracing experiments contain an overlapping population of starter cells. However, these Tph2+Gad2+ cells are a small fraction of the population, making it unlikely that they would alter our conclusions. A third limitation is that our study samples large populations of starter cells across the DR, which likely combine many distinct subpopulations of DR neurons (discussed below). From these caveats and limitations, we suggest that this study of inputs to populations of DR neurons has reliably revealed trends and biases that likely underestimate the true specificity within DR circuits.

DR Neurons Receive Diverse Inputs

Our results are consistent with previous DR input studies using classic tracers (reviewed in Hornung, 2010; Jacobs and Azmitia, 1992). As a specific example, a comprehensive retrograde tracing study in the rat (Peyron et al., 1998) labeled cells in all of the forebrain areas that we identified as sending input to the DR. Our study has extended these previous studies by enabling us to identify the presynaptic partners of specific DR cell types. We found that the major input regions are often associated with processing autonomic and emotional information, such as the amygdala, hypothalamic subregions, and LHb (Swanson, 2011; Lammel et al., 2012; Matsumoto and Hikosaka, 2009). Additional input regions include the anterior cortex and cerebellar nuclei that play diverse roles in coordinating sensation and action, motor control, and cognitive function (Swanson, 2011).

This study treated the DR as a homogenous unit for the purpose of characterizing its overall input. Previous studies (see Introduction) and data presented here (Figures 6F, 7, and 8) suggest that these results likely represent input to starter cells that consist of multiple subtypes that receive unique combinations of inputs. We also observed that input regions were differentially variable (Figures 3, 5, and 8). This differential variability suggests that highly variable input regions innervate specific cell populations that are particularly sensitive to starter cell selection, while less variable regions may more widely innervate the DR or target less clustered populations. These highly variable input regions are exciting candidates for the dissection of functional subcircuits.

Cortical Inputs to the DR

Our map of long-range inputs has identified interesting differences between DR serotonin and GABA neurons (Figure 8F). Among inputs to the DR, medial prefrontal cortex (mPFC) has received particular attention (mPFC is mostly composed of our PrL/Cg and infralimbic subdivisions) (Figure 5). Stimulation of the rat mPFC causes a reduction in the firing rates of DR serotonin neurons in vivo (Celada et al., 2001; Hajós et al., 1998), suggesting that mPFC axons mainly synapse onto DR GABA neurons, which in turn inhibit serotonin neurons. In support of this hypothesis, an electron microscopic (EM) study using dual labeling of mPFC afferents and Tph2 (serotonergic neurons) or GABA found more frequent mPFC terminals synapsing onto GABA-labeled dendrites than Tph2-labeled dendrites (Jankowski and Sesack, 2004). Our study found that cortical subregions (including the PrL/Cg) were preferentially labeled when starter cells were DR serotonin neurons rather than GABA neurons, and our CRACM analysis found that serotonin neurons had a 2-fold higher chance of receiving input from the anterior cortex as a whole when compared to GABA neurons.

Differences in the techniques used (and the subsequent conclusions) in our study and these previous ones may provide insight into DR circuit structure. It is clear from this combination of studies that mPFC projections synapse onto both serotonin and GABA neurons. The bias found in the EM study (Jankowski and Sesack, 2004) when compared to ours suggests that rates of cortical input to DR cell types vary across DR and/or cortical subregions. This is consistent with our observation that specific cortical subregions make up a larger fraction of input to DR serotonin neurons compared to GABA neurons (notably not the infralimbic cortex) (Figure 5B). Further, GABA neurons receiving cortical input are clustered in a specific portion of the DR, within which the connectivity rate is comparable to that observed for serotonin neurons overall (Figure 6F). Interestingly, the inhibition of DR serotonin neurons by mPFC stimulation observed in Celada et al. (2001) was in part due to activation of inhibitory serotonin autoreceptors, consistent with local tracing that identified extensive interconnectivity of DR serotonin neurons (Figure 7). We therefore suggest the following: (1) cortical inputs to the DR, taken overall, preferentially synapse onto serotonin neurons; (2) connectivity rates are highly variable over subregions of the DR and cortex; and (3) cortical inputs to the DR interact with a complex local circuit that may feature substantial serotonergic local inhibition.

On the Relationship between DR Serotonin and GABA Neurons

Several possibilities could account for the finding that DR serotonin and GABA neurons receive inputs from the same regions. It is possible that specificity is diluted due to the technical caveats described above. However, the coinnervation of serotonin and GABA neurons may reflect complex computations by the local DR circuit and a need to control serotonin activity in a spatiotemporally precise manner. For example, excitation of a population of serotonin neurons may be accompanied by inhibition of other serotonin neurons locally, or followed by inhibition of the same serotonin neurons to limit the duration of excitation, akin to lateral inhibition and feedforward inhibition in many other systems (Isaacson and Scanziani, 2011). Feedforward inhibition may contribute to the low firing rates of serotonin neurons (Jacobs and Azmitia, 1992; Urbain et al., 2006).

Whereas GABA neurons in the DR are generally thought to locally inhibit serotonin neurons, our local tracing studies revealed spatial selectivity of the direct GABAergic input to serotonin neurons. We identified a subregion of the midbrain reticular nucleus, ventral to the periaqueductal gray, as a particularly strong source of GABAergic input to DR serotonin neurons. By comparison, the GABA neurons in the dorsal and ventral wings within the periaqueductal gray are not as

enriched. Conditional to the caveats of rabies tracing, this suggests that many local GABA neurons may not directly synapse onto DR serotonin neurons. Several possibilities may account for this. First, some GABA neurons may act mainly on the presynaptic terminals of neurons that synapse onto serotonin or other DR neurons (Soiza-Reilly et al., 2013). Second, some GABA neurons may inhibit other GABA neurons or other local neurons such as glutamate and dopamine neurons. Third, many DR GABA neurons are known to send long-range projections (Bang and Commons, 2012). Given the abundant long-range GABAergic projections from the DR, it is intriguing to consider the DR as two parallel but interacting subsystems that integrate similar inputs and send either serotonergic or GABAergic outputs. Data presented here suggest that DR GABA neurons are particularly heterogeneous and may therefore be ideal first targets for further dissection of DR function.

We hope that this map of synaptic input to serotonin and GABA neurons with respect to brain areas, neurotransmitter phenotypes, and synaptic properties will serve as a foundation for future functional interrogation of specific DR pathways.

EXPERIMENTAL PROCEDURES

All animal procedures followed animal care guidelines approved by Stanford University's Administrative Panel on Laboratory Animal Care (APLAC). All handling of rabies virus followed procedures approved by Stanford University's Administrative Panel on Biosafety (APB) for Biosafety Level 2.

Mice and Anatomical Regions

Four *Sert-cre* and four *Gad2-cre* brains were chosen based on high tracing efficiency and starter cells largely restricted to the DR. The DR clusters of serotonin and GABA neurons are in close apposition to those of the rostral- and central-linear raphe nucleus (RLi, CLi), which is directly ventral to the DR at certain planes, as well as the midbrain reticular nucleus (MRtN). These experiments included starter cells in these regions, but we excluded brains with significant starter cells in other regions, particularly the VTA and median raphe (Figures S3 and S4). These brains were chosen from seven *Sert-cre* and 11 *Gad2-cre* tracing experiments, not including TC^{66T} experiments and brains for ISH, which were processed differently (see Supplemental Experimental Procedures). For the replication cohort, three *Sert-cre* and four *Gad2-cre* experiments were selected from five additional injections. Each included one brain from the original seven *Sert-cre* and 11 *Gad2-cre* that had not been chosen as one of the original eight but was still restricted in starter cells and efficient in transsynaptic spread.

For quantifications of subregions, boundaries were based on the Allen Institute's reference atlas (Lein et al., 2007) with consultation of Paxinos and Franklin (2001). The EAM is treated particularly differently in these two atlases (Heimer et al., 1997). According to the Allen atlas, our definition includes the substantia innominata, magnocellular nucleus, anterior amygdalar area, and the fundus of striatum, though we often used Paxinos and Franklin (2001) to adjust borders around subregions not annotated in the Allen atlas, such as the interstitial nucleus of the posterior limb of the anterior commissure (IPAC). The infralimbic cortex and medulla are as defined in the Allen atlas, though for medulla, sections anterior to the appearance of the DR were omitted due to possible local background (Figure S1). For counts of thalamic subregions, we were conservative while counting sections that border midbrain nuclei, so our counts may underestimate posterior thalamic subregions. For all regions except the BNST, arcuate nucleus, DMH, and VMH, every third section was counted, and the final number is adjusted by a factor of three. These four exceptions are relatively small and rapidly changing regions, so every second section was counted to get a more accurate estimate, and the final number was adjusted by a factor of two. Note that we did not adjust for the possibility of double counting cells, which likely results in overestimates, with the extent depending on the size of the cells in the regions quantified.

Statistical Analysis

For long-range tracing data, cell counts for each experiment were first normalized to the lowest efficiency tracing experiment (2,697 total cells) so that the total number of cells in each brain was equal. As most of the variance could be accounted for by the number of cells in a region (R^2 = 0.85 for *Sert-cre* and R^2 = 0.73 for *Gad2-cre*), we took the logarithm of the number of cells in each region, which allowed us to perform two-way ANOVA as the variances were equal across regions (Brown-Forsythe test). Normality was confirmed with the D'Agostino and Pearson test. All p values for subregion post hoc tests were corrected against all of the subregions included in the analysis (those that contained less than 1% of total labeling were omitted).

Analysis of local subregion inputs in Figure 7 used one-way ANOVA followed by Bonferroni corrections (equal SD, Brown-Forsythe test). All graphing and analysis described above was done using Prism software (GraphPad). For analysis of clustering in Figure 8, we created a vector for each experimental brain containing the proportions of GFP+ cells in each subregion. We then generated pairwise correlations in Matlab (Mathworks) and graphed relationships using Prism (GraphPad). Heatmaps and dendrograms were generated in R (http://www.r-project.org/).

Supplemental Experimental Procedures contain detailed descriptions of rabies-mediated transsynaptic tracing, rabies tracing combined with in situ hybridization (ISH), histology and imaging, PCR primers used to prepare templates for ISH probes, and CRACM.

SUPPLEMENTAL INFORMATION

Supplemental Information includes seven figures, one table, and Supplemental Experimental Procedures and can be found with this article online at http://dx.doi.org/10.1016/j.neuron.2014.06.024.

ACKNOWLEDGMENTS

We thank R. Malenka for advice on electrophysiology; M. Lochrie and The Stanford Viral Core for AAV production; T. Mosca for help with image analysis; X. Gao, C. Lowe, and W. Allen for advice on data analysis; C. Manalac for technical support; and R. Malenka, L. Swanson, B. Grone, E. Rose, E. Williams, and members of the Luo Lab for discussions and critiques on the manuscript. We thank N. Uchida and K. Meletis for coordinating submission. B.C.W. is supported by a Stanford Graduate Fellowship and an NSF Graduate Research Fellowship (grant number DGE-114747). C.J.G. was supported by a National Defense Science and Engineering Graduate Fellowship. K.M. was a Research Specialist, and L.L. is an Investigator, of the Howard Hughes Medical Institute. Supported by an HHMI Collaborative Innovation Award (HCIA).

Accepted: June 19, 2014
Published: August 6, 2014

REFERENCES

Amat, J., Baratta, M.V., Paul, E., Bland, S.T., Watkins, L.R., and Maier, S.F. (2005). Medial prefrontal cortex determines how stressor controllability affects behavior and dorsal raphe nucleus. Nat. Neurosci. *8*, 365–371.

Bang, S.J., and Commons, K.G. (2012). Forebrain GABAergic projections from the dorsal raphe nucleus identified by using GAD67-GFP knock-in mice. J. Comp. Neurol. *520*, 4157–4167.

Bargmann, C.I., and Marder, E. (2013). From the connectome to brain function. Nat. Methods *10*, 483–490.

Belin, M.F., Nanopoulos, D., Didier, M., Aguera, M., Steinbusch, H., Verhofstad, A., Maitre, M., and Pujol, J.F. (1983). Immunohistochemical evidence for the presence of gamma-aminobutyric acid and serotonin in one nerve cell. A study on the raphe nuclei of the rat using antibodies to glutamate decarboxylase and serotonin. Brain Res. *275*, 329–339.

Bockaert, J., Claeysen, S.A.D., and Marin, P. (2010). Classification and signaling characteristics of 5-HT receptors. In Handbook of Behavioral Neurobiology of Serotonin, C.P. Müller and B.L. Jacobs, eds. (Elsevier).

Brunelli, M., Castellucci, V., and Kandel, E.R. (1976). Synaptic facilitation and behavioral sensitization in Aplysia: possible role of serotonin and cyclic AMP. Science *194*, 1178–1181.

Calizo, L.H., Akanwa, A., Ma, X., Pan, Y.Z., Lemos, J.C., Craige, C., Heemstra, L.A., and Beck, S.G. (2011). Raphe serotonin neurons are not homogenous: electrophysiological, morphological and neurochemical evidence. Neuropharmacology *61*, 524–543.

Celada, P., Puig, M.V., Casanovas, J.M., Guillazo, G., and Artigas, F. (2001). Control of dorsal raphe serotonergic neurons by the medial prefrontal cortex: Involvement of serotonin-1A, GABA(A), and glutamate receptors. J. Neurosci. *21*, 9917–9929.

Dahlström, A., and Fuxe, K. (1964). Evidence for the existence of monoamine containing neurons in the central nervous system, I. Demonstration of monoamines in the cell bodies of brain stem neurons. Acta Physiol. Scand. *62* (suppl. 232), 1–55.

Descarries, L., Watkins, K.C., Garcia, S., and Beaudet, A. (1982). The serotonin neurons in nucleus raphe dorsalis of adult rat: a light and electron microscope radioautographic study. J. Comp. Neurol. *207*, 239–254.

Descarries, L., Riad, M., and Parent, M. (2010). Ultrastructure of the serotonin innervation in the mammalian central nervous system. In Handbook of Behavioral Neurobiology of Serotonin, C.P. Müller and B.L. Jacobs, eds. (Elsevier).

Gaspar, P., Cases, O., and Maroteaux, L. (2003). The developmental role of serotonin: news from mouse molecular genetics. Nat. Rev. Neurosci. *4*, 1002–1012.

Gong, S., Doughty, M., Harbaugh, C.R., Cummins, A., Hatten, M.E., Heintz, N., and Gerfen, C.R. (2007). Targeting Cre recombinase to specific neuron populations with bacterial artificial chromosome constructs. J. Neurosci. *27*, 9817–9823.

Hajós, M., Richards, C.D., Székely, A.D., and Sharp, T. (1998). An electrophysiological and neuroanatomical study of the medial prefrontal cortical projection to the midbrain raphe nuclei in the rat. Neuroscience *87*, 95–108.

Hale, M.W., and Lowry, C.A. (2011). Functional topography of midbrain and pontine serotonergic systems: implications for synaptic regulation of serotonergic circuits. Psychopharmacology *213*, 243–264.

Hale, M.W., Shekhar, A., and Lowry, C.A. (2012). Stress-related serotonergic systems: implications for symptomatology of anxiety and affective disorders. Cell. Mol. Neurobiol. *32*, 695–708.

Haubensak, W., Kunwar, P.S., Cai, H., Ciocchi, S., Wall, N.R., Ponnusamy, R., Biag, J., Dong, H.W., Deisseroth, K., Callaway, E.M., et al. (2010). Genetic dissection of an amygdala microcircuit that gates conditioned fear. Nature *468*, 270–276.

Heimer, L., Harlan, R.E., Alheid, G.F., Garcia, M.M., and de Olmos, J. (1997). Substantia innominata: a notion which impedes clinical-anatomical correlations in neuropsychiatric disorders. Neuroscience *76*, 957–1006.

Hornung, J.P. (2010). The neuroanatomy of the serotonergic system. In Handbook of Behavioral Neurobiology of Serotonin, C.P. Müller and B.L. Jacobs, eds. (Elsevier).

Isaac, J.T., Ashby, M.C., and McBain, C.J. (2007). The role of the GluR2 subunit in AMPA receptor function and synaptic plasticity. Neuron *54*, 859–871.

Isaacson, J.S., and Scanziani, M. (2011). How inhibition shapes cortical activity. Neuron *72*, 231–243.

Jacobs, B.L., and Azmitia, E.C. (1992). Structure and function of the brain serotonin system. Physiol. Rev. *72*, 165–229.

Jankowski, M.P., and Sesack, S.R. (2004). Prefrontal cortical projections to the rat dorsal raphe nucleus: ultrastructural features and associations with serotonin and gamma-aminobutyric acid neurons. J. Comp. Neurol. *468*, 518–529.

Kirby, L.G., Pernar, L., Valentino, R.J., and Beck, S.G. (2003). Distinguishing characteristics of serotonin and non-serotonin-containing cells in the dorsal raphe nucleus: electrophysiological and immunohistochemical studies. Neuroscience *116*, 669–683.

Lammel, S., Lim, B.K., Ran, C., Huang, K.W., Betley, M.J., Tye, K.M., Deisseroth, K., and Malenka, R.C. (2012). Input-specific control of reward and aversion in the ventral tegmental area. Nature *491*, 212–217.

Lasaga, M., and Debeljuk, L. (2011). Tachykinins and the hypothalamo-pituitary-gonadal axis: An update. Peptides *32*, 1972–1978.

Lein, E.S., Hawrylycz, M.J., Ao, N., Ayres, M., Bensinger, A., Bernard, A., Boe, A.F., Boguski, M.S., Brockway, K.S., Byrnes, E.J., et al. (2007). Genome-wide atlas of gene expression in the adult mouse brain. Nature *445*, 168–176.

Liu, Y., Jiang, Y., Si, Y., Kim, J.Y., Chen, Z.F., and Rao, Y. (2011). Molecular regulation of sexual preference revealed by genetic studies of 5-HT in the brains of male mice. Nature *472*, 95–99.

Maier, S.F., and Watkins, L.R. (2005). Stressor controllability and learned helplessness: the roles of the dorsal raphe nucleus, serotonin, and corticotropin-releasing factor. Neurosci. Biobehav. Rev. *29*, 829–841.

Matsumoto, M., and Hikosaka, O. (2009). Representation of negative motivational value in the primate lateral habenula. Nat. Neurosci. *12*, 77–84.

Miyamichi, K., Amat, F., Moussavi, F., Wang, C., Wickersham, I., Wall, N.R., Taniguchi, H., Tasic, B., Huang, Z.J., He, Z., et al. (2011). Cortical representations of olfactory input by trans-synaptic tracing. Nature *472*, 191–196.

Miyamichi, K., Shlomai-Fuchs, Y., Shu, M., Weissbourd, B.C., Luo, L., and Mizrahi, A. (2013). Dissecting local circuits: parvalbumin interneurons underlie broad feedback control of olfactory bulb output. Neuron *80*, 1232–1245.

Müller, C.P., and Jacobs, B.L. (2010). Handbook of the Behavioral Neurobiology of Serotonin. (Elsevier).

Nestler, E., Hyman, S., and Makenka, R. (2009). Molecular Neuropharmacology: A Foundation for Clinical Neuroscience, Second Edition. (McGraw-Hill).

Paxinos, G., and Franklin, K.B.J. (2001). The Mouse Brain. In Stereotaxic Coordinates, Second EditionStereotaxic Coordinates (Academic Press).

Petreanu, L., Huber, D., Sobczyk, A., and Svoboda, K. (2007). Channelrhodopsin-2-assisted circuit mapping of long-range callosal projections. Nat. Neurosci. *10*, 663–668.

Peyron, C., Petit, J.M., Rampon, C., Jouvet, M., and Luppi, P.H. (1998). Forebrain afferents to the rat dorsal raphe nucleus demonstrated by retrograde and anterograde tracing methods. Neuroscience *82*, 443–468.

Sawin, E.R., Ranganathan, R., and Horvitz, H.R. (2000). C. elegans locomotory rate is modulated by the environment through a dopaminergic pathway and by experience through a serotonergic pathway. Neuron *26*, 619–631.

Shikanai, H., Yoshida, T., Konno, K., Yamasaki, M., Izumi, T., Ohmura, Y., Watanabe, M., and Yoshioka, M. (2012). Distinct neurochemical and functional properties of GAD67-containing 5-HT neurons in the rat dorsal raphe nucleus. J. Neurosci. *32*, 14415–14426.

Soiza-Reilly, M., Anderson, W.B., Vaughan, C.W., and Commons, K.G. (2013). Presynaptic gating of excitation in the dorsal raphe nucleus by GABA. Proc. Natl. Acad. Sci. USA *110*, 15800–15805.

Stepien, A.E., Tripodi, M., and Arber, S. (2010). Monosynaptic rabies virus reveals premotor network organization and synaptic specificity of cholinergic partition cells. Neuron *68*, 456–472.

Swanson, L.W. (2011). Brain Architecture: Understanding the Basic Plan. (Oxford: Oxford University Press).

Takatoh, J., Nelson, A., Zhou, X., Bolton, M.M., Ehlers, M.D., Arenkiel, B.R., Mooney, R., and Wang, F. (2013). New modules are added to vibrissal premotor circuitry with the emergence of exploratory whisking. Neuron *77*, 346–360.

Taniguchi, H., He, M., Wu, P., Kim, S., Paik, R., Sugino, K., Kvitsiani, D., Fu, Y., Lu, J., Lin, Y., et al. (2011). A resource of Cre driver lines for genetic targeting of GABAergic neurons in cerebral cortex. Neuron *71*, 995–1013.

Ugolini, G. (1995). Specificity of rabies virus as a transneuronal tracer of motor networks: transfer from hypoglossal motoneurons to connected second-order and higher order central nervous system cell groups. J. Comp. Neurol. *356*, 457–480.

Urbain, N., Creamer, K., and Debonnel, G. (2006). Electrophysiological diversity of the dorsal raphe cells across the sleep-wake cycle of the rat. J. Physiol. *573*, 679–695.

Walker, F.R. (2013). A critical review of the mechanism of action for the selective serotonin reuptake inhibitors: do these drugs possess anti-inflammatory properties and how relevant is this in the treatment of depression? Neuropharmacology *67*, 304–317.

Warden, M.R., Selimbeyoglu, A., Mirzabekov, J.J., Lo, M., Thompson, K.R., Kim, S.Y., Adhikari, A., Tye, K.M., Frank, L.M., and Deisseroth, K. (2012). A prefrontal cortex-brainstem neuronal projection that controls response to behavioural challenge. Nature *492*, 428–432.

Watabe-Uchida, M., Zhu, L., Ogawa, S.K., Vamanrao, A., and Uchida, N. (2012). Whole-brain mapping of direct inputs to midbrain dopamine neurons. Neuron *74*, 858–873.

Wickersham, I.R., Lyon, D.C., Barnard, R.J., Mori, T., Finke, S., Conzelmann, K.K., Young, J.A., and Callaway, E.M. (2007). Monosynaptic restriction of transsynaptic tracing from single, genetically targeted neurons. Neuron *53*, 639–647.

Neuron, Volume *83*

Supplemental Information

Presynaptic Partners of Dorsal Raphe Serotonergic and GABAergic Neurons

Brandon Weissbourd, Jing Ren, Katherine E. DeLoach, Casey J. Guenthner, Kazunari Miyamichi, and Liqun Luo

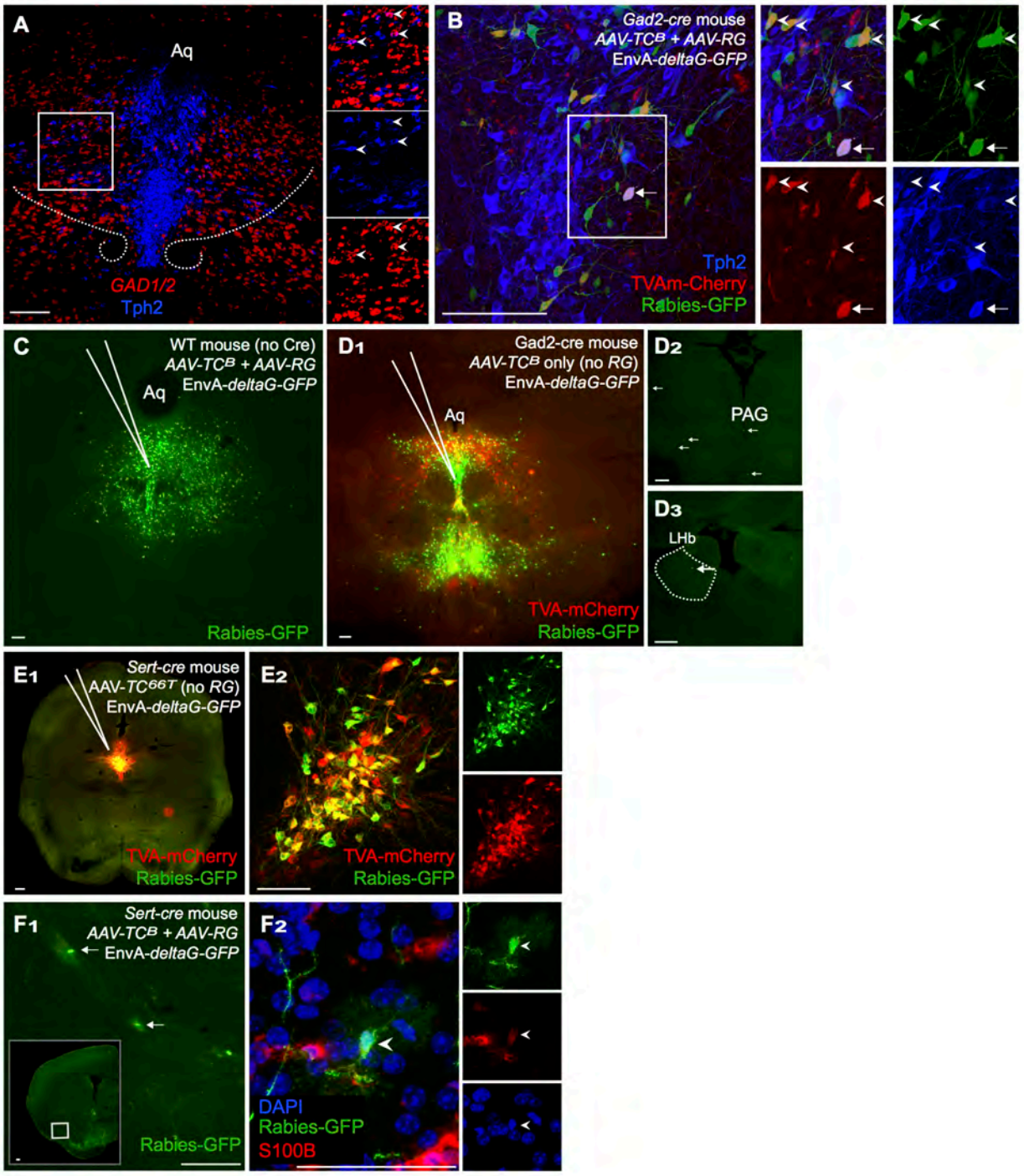

Figure S1. Characterization of Starter Cell Populations and Rabies Tracing, related to Figure 1.

(A) Double labeling of Tph2 antibody staining (blue) and *Gad1/2* in situ (red) showing serotonin and GABA neurons in the DR, which are mostly distributed in complementary patterns. However, particularly in the lateral wings, there is substantial intermingling of these two types of neurons (see high magnification of the boxed area on the right). Occasionally double-labeled cells were found (three double-labeled cells in this image are indicated with arrowheads). Aq: aqueduct.

(B) In this *Gad2-cre* tracing mouse, starter cells at the DR (mCherry+ GFP+) were co-stained with anti-Tph2 antibody. While the vast majority of starter cells were Tph2-negative (arrowheads), ~5% of starter cells were Tph2-positive (arrow).
(C) In this control experiment, the DR of wild-type mice (with no Cre expression) was transduced with AAV5 *CAG-FLEx-TC^{B}*/AAV8 *CAG-FLEx-RG* followed by infection with EnvA-pseudotyped, RG-deleted, and GFP-expressing rabies virus (see Figure 1B). Significant local background infection by rabies virus was observed (green cells, 1465±1132, mean ± SEM, n=4) but minimal long-range (10.75±6.5 total cells in forebrain). Data reported in Miyamichi et al. (2013), as well as data from panel F below, indicate that this was caused by Cre-independent leaky expression of TVA from the AAV *CAG-FLEx-TC^{B}*, allowing rabies infection (since trace amounts of TVA expression can result in rabies infection, the expression of mCherry from TVA-mCherry is not necessarily visible.) Thus, the *TC^{B}* strategy is not suitable for tracing local input. Image shown is from the experiment with the highest background observed.
(D) In this control experiment, the DR and surrounding regions of a *Gad2-cre* mouse was transduced with AAV5 *CAG-FLEx-TC^{B}* without AAV8 *CAG-FLEx-RG*, followed by infection with EnvA-pseudotyped, RG-deleted, and GFP-encoding rabies virus. The presence of TC^{B} should allow initial rabies infection, but the absence of RG should prevent spread of rabies-GFP to presynaptic cells. (D_1) Local GFP+/TVA-mCherry-negative cells are likely caused by leaky expression of TVA as in (C). (D_2-D_3) Sparse long-range GFP+ cells were observed with decreasing frequency per section further from the DR (2.3±0.6 cells per section on average in the forebrain). (D_2) shows labeling (arrows) in anterior midbrain nuclei (PAG, periaqueductal grey) and (D_3) shows labeling in the lateral habenula (LHb). Images shown are from the experiment with the highest background observed. This long-range background is likely caused by retrograde transport of AAV-*TC^{B}* in neurons that project axons to the DR from their axon terminals, followed by rabies virus infection. This observation of long-range background is different from what we had previously observed using different experimental conditions (Miyamichi et al., 2013). This is likely due to the difference in serotype used for AAV *CAG-FLEx-TC^{B}* in this study (serotype 5 instead of serotype 2, which was used in Miyamichi et al., 2013). Alternatively, retrograde AAV infection could also be enhanced by specific characteristics of the DR neurons compared to the cortical and olfactory bulb neurons analyzed in previous studies. Compared to the high efficiency of Cre-dependant *TC^{B}* tracing (many thousands of cells, see Figure 2), this long-range background is negligible outside of the area surrounding the DR, which we did not include in our TC^{B} tracing analysis. In summary, we conclude from these control experiments that TC^{B}-based tracing is suitable for tracing long-range but not local input.
(E) In this control experiment, *Sert-cre* mice were transduced with AAV2 *CAG-FLEx-TC^{66T}* (mutant TVA receptor with 10-fold lower affinity to EnvA) without AAV8 *CAG-FLEx-RG*, followed by infection with EnvA-pseudotyped, RG-deleted and GPF-encoding rabies virus. Unlike the analogous experiment in panel D_1, all GFP+ cells are also mCherry+ within the DR (E_1) as examined by confocal microscopy at high magnification (E_2), with GFP+/TVA-mCherry- cells being rare to nonexistent in three mice treated under the same conditions described above. In five additional wild-type mice, we transduced AAV2 *CAG-FLEx-TC^{66T}*/AAV8 *CAG-FLEx-RG* followed by EnvA-pseudotyped, RG-deleted and GFP-encoding rabies virus (analogous to the control experiment shown in panel C; data not shown). Labeled cells were never observed in these control experiments. Thus, we conclude that *TC^{66T}*-based tracing can be applied to tracing local input with minimal background.

(F) When analyzing our long range tracing data, we also observed what appeared to be GFP-labeled glial cells based on morphology (arrows in F_1, which is a high magnification of the boxed region in the inset) and S100B antibody staining (arrowhead, F_2). These glial cells often appear around axon tracts, particularly the external capsule. This phenomenon may be due to an immune response to rabies infection. As there were no obvious differences in the distributions of inputs between brains with and without labeled glia, we did not exclude brains with GFP+ glia. Scale: 200 μm.

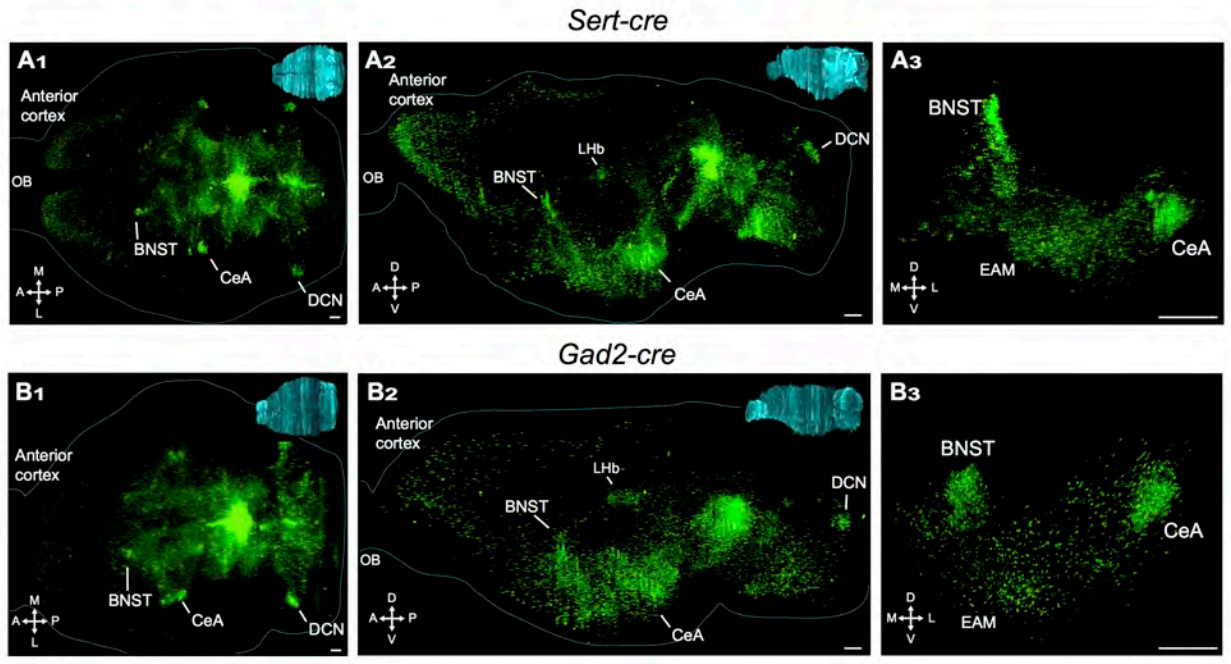

Figure S2. 3D-rendering of Long-range Inputs to the DR, related to Figure 2.
(A and B) Horizontal (A_1, B_1) and sagittal bisected (A_2, B_2) views of 3D reconstructed brains from Figure 2 showing overall distributions of input neurons to DR serotonin neurons (A) and GABA neurons (B) from different perspectives. The cyan images on the top right show the same brain counterstained with NeuroTrace Blue, which was used to register the 2D sections into the 3D volume, and rough brain outlines are drawn in cyan based on those images. A_3 and B_3 are high magnification rotated coronal views highlighting the continual distribution of input neurons in extended amygdala from BNST to CeA in *Sert-cre* (A_3) and *Gad2-cre* (B_3) experiments. Scale: 400 μm. Abbreviations: OB: olfactory bulb, BNST: bed nucleus of the stria terminalis, CeA: central amygdala, DCN: deep cerebellar nuclei, LHb: lateral habenula, EAM: extended amygdala.

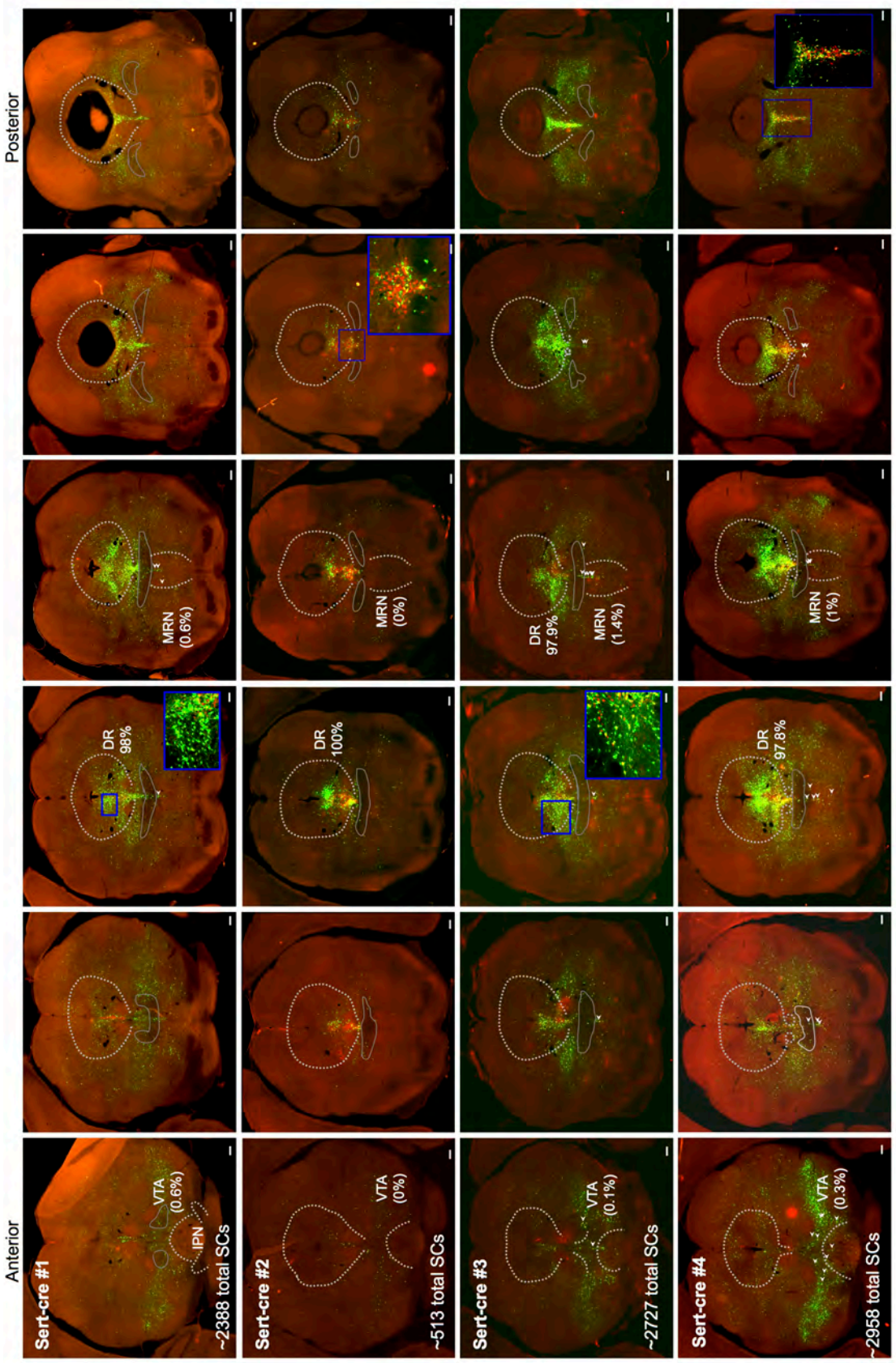
Anterior
Posterior
Sert-cre #1
VTA (0.6%)
IPN
~2388 total SCs
DR 98%
MRN (0.6%)
Sert-cre #2
VTA (0%)
~513 total SCs
DR 100%
MRN (0%)
Sert-cre #3
VTA (0.1%)
~2727 total SCs
DR 97.9%
MRN (1.4%)
Sert-cre #4
VTA (0.3%)
~2958 total SCs
DR 97.8%
MRN (1%)

Figure S3. Starter Cell Distributions of the 4 Experiments used for Long-range Tracing of Inputs to DR Serotonin Neurons, Related to Figure 2.

Each row represents one *Sert-cre* tracing brain; the 6 columns represent 6 coronal sections from anterior to posterior across DR. Starter cells are double labeled by TVA-mCherry and rabies-GFP, and therefore are yellow. Indicated are estimated total starter cell numbers and % starter cells that are confined to DR (as defined in Figure 1A), VTA (ventral tegmental area), and MRN (median raphe nucleus). Starter cells in the MRN, interpeduncular nucleus (IPN), and VTA indicated with arrowheads. Selected regions (blue rectangles) are magnified in insets. Scale: 250 μm.

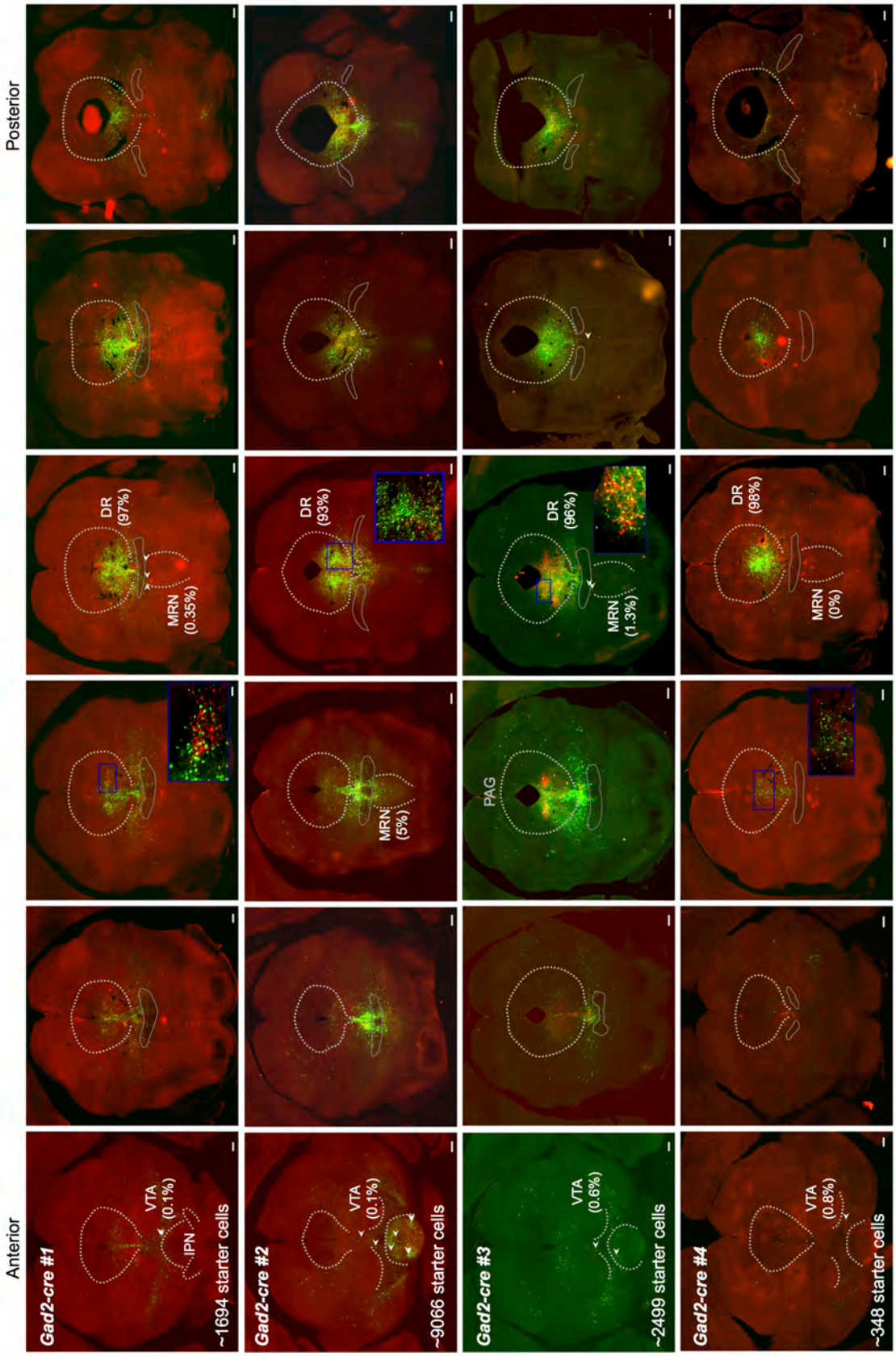
Anterior
Posterior
Gad2-cre #1
VTA (0.1%)
IPN
~1694 starter cells
DR (97%)
MRN (0.35%)
Gad2-cre #2
VTA (0.1%)
~9066 starter cells
MRN (5%)
Gad2-cre #3
VTA (0.6%)
~2499 starter cells
PAG
DR (96%)
MRN (1.3%)
Gad2-cre #4
VTA (0.8%)
~348 starter cells
DR (98%)
MRN (0%)
DR (93%)

Figure S4. Starter Cell Distributions of the 4 Experiments used for Long-range Tracing of Inputs to DR GABA Neurons, Related to Figure 2.

Each row represents one *Gad2-cre* tracing brain; the 6 columns represent 6 coronal sections from anterior to posterior across DR. Starter cells are double labeled by TVA-mCherry and rabies-GFP, and therefore are yellow. Indicated are estimated total starter cell numbers and % starter cells that are confined to DR (as defined in Figure 1A), VTA (ventral tegmental area), and MRN (median raphe nucleus). Starter cells in the MRN, interpeduncular nucleus (IPN), and VTA indicated with arrowheads, except in *Gad2-cre* #2. Selected regions (blue rectangles) are magnified in insets. Scale: 250 μm.

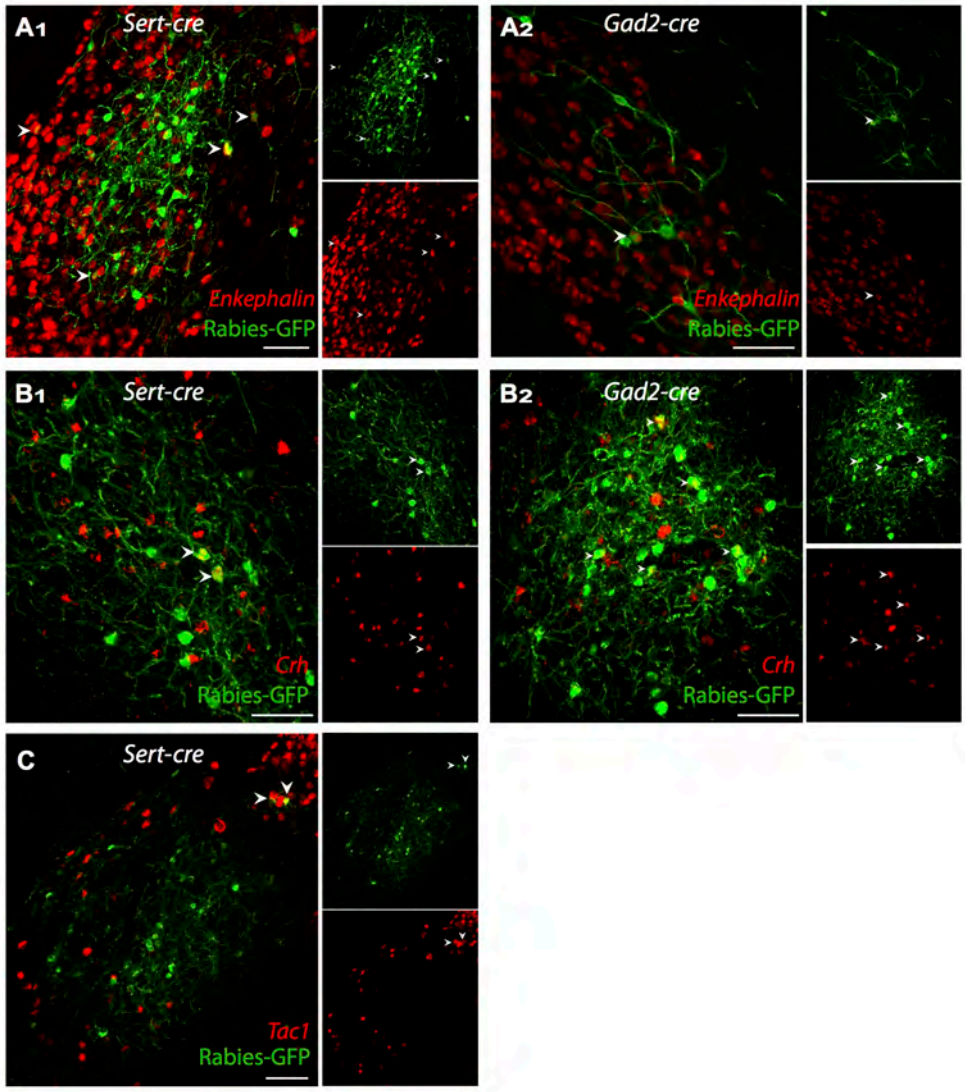

Figure S5. Peptidergic Inputs from the Central Amygdala to DR Serotonin and GABA Neurons, related to Figure 4.

(A) Sparse inputs from the central amygdala (CeA) to DR serotonin (A_1) and GABA (A_2) neurons from cells expressing *preproenkephalin*. Arrows indicate double-positive cells. Red: *preproenkephalin* ISH, green: rabies-GFP. Based on n=1 *Sert-cre* tracing brain and n=1 *Gad2-cre* tracing brain.

(B) Inputs from the central amygdala (CeA) to DR serotonin (B_1) and GABA (B_2) neurons overlap with cells expressing *corticotropin releasing hormone* (*Crh)*. Arrows indicate double-positive cells. Red: *Crh* ISH, green: rabies-GFP. In 8 sectioning planes of the central amygdala an average of 15% and 25% of input neurons from 1 *Sert-cre* 1 *Gad2-cre* tracing brain, respectively, were *Crh*+, with considerable variation across CeA subregions.

(C) Sparse inputs from the central amygdala (CeA) to DR serotonin neurons from cells expressing *Tac1*. Arrows indicate double-positive cells. Red: *Tac1* ISH, green: rabies-GFP. Based on n=1 *Sert-cre* tracing brain.

Scale: 100 μm.

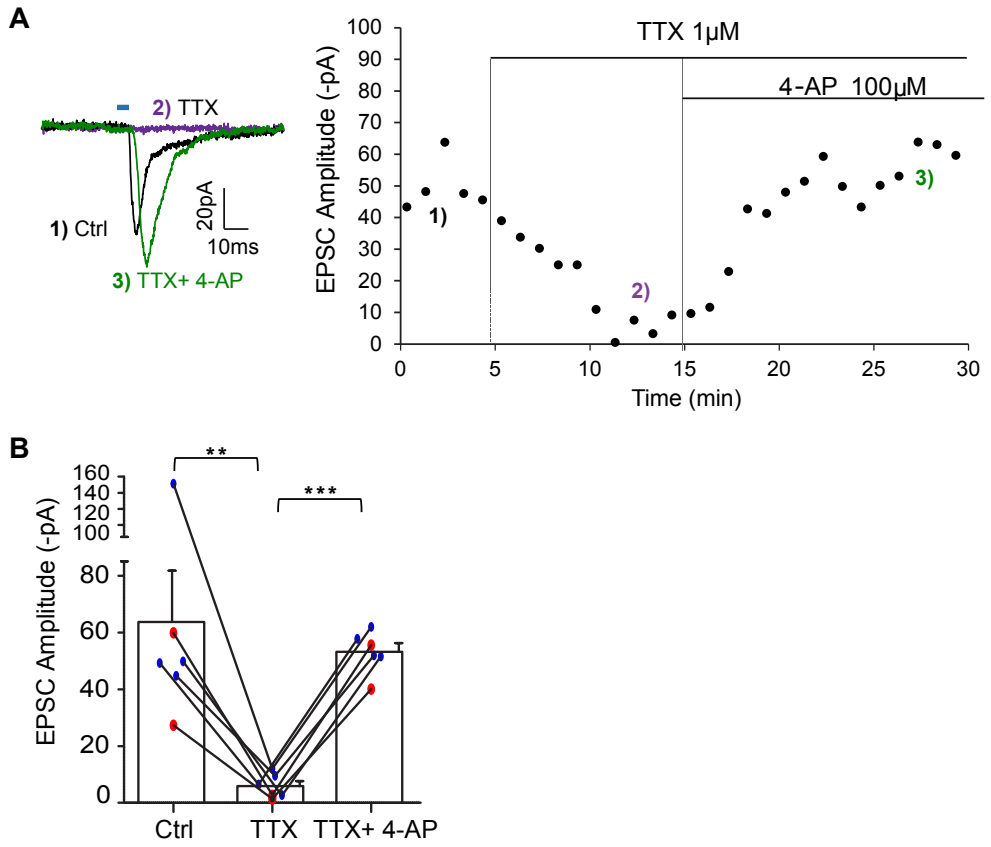

Figure S6 DR Neurons receive Monosynaptic Input from Anterior Cortex, related to Figure 6.

(A) Left, a representative DR neuron showing that 5-ms photostimulation-evoked fast EPSCs (A_1, control (Ctrl), black trace). The average latency of evoked EPSCs (from the onset of the laser command to the rise of EPSCs) is 5.74±1.61ms (n=24), which is consistent with the connections between ChR2-EYFP fibers and DR neurons being monosynaptic and excitatory (see discussion in Petreanu et al., 2007). Application of 1 μM TTX eliminated evoked EPSCs (A_2, purple trace). Addition of 100 μM 4-AP restored evoked EPSCs (A_3, green trace). This is consistent with monosynaptic connections. (TTX blocks action potential propagation, which is required for synaptic transmission for both mono- and poly-synaptic connections under physiological conditions. ChR2-induced depolarization alone is insufficient to induce synaptic transmission in the presence of TTX. However, 4-AP can augment ChR2-induced depolarization of synaptic terminals in the presence of TTX, allowing for synaptic transmission only under mono-synaptic conditions; see Petreanu et al., 2009; Holloway et al., 2013). Compared to the light-evoked EPSCs before drug application, the onset latency of these events were typically delayed (9.72±0.8ms vs 5.10±0.5ms; p = 0.00057, paired t test) and they were broader (decay time constant, 21.8±3.8ms vs 11.3±2.1ms; p = 0.0046), consistent with other optogenetic studies (Holloway et al., 2013). Trace samples are the average of 6 trials from the same neuron, with 20s inter-trial intervals. Right, change of EPSCs amplitude over time. Each dot presents the average of EPSCs over 1min.

(B) Group data from 6 cells showing that the addition of 4-AP almost fully restored the TTX inhibition, suggesting monosynaptic input from anterior cortical projection neurons. Blue dots, serotonin neurons. Red dots, GABA neurons. Paired t-test, n=6 cells).

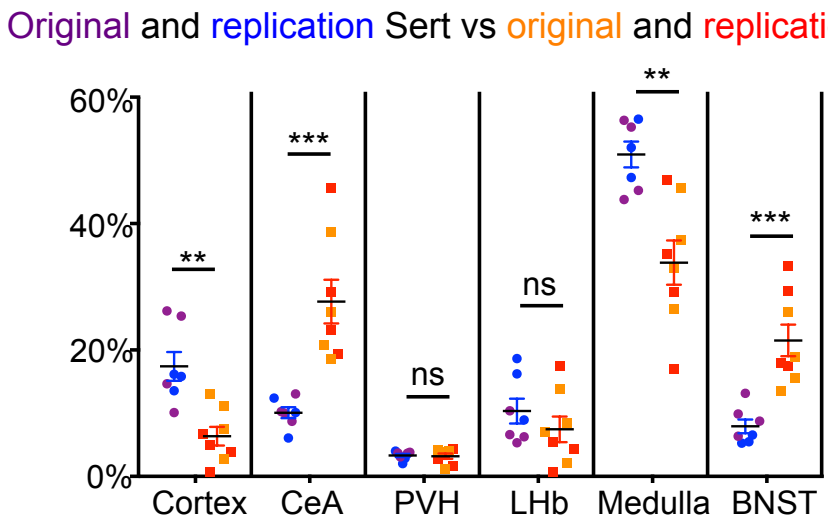

Figure S7 Validation of Selected Input Regions with an Independent Cohort, Related to Figure 8.

Quantification of 6 subregions in a replication cohort of 3 *Sert-cre* (purple) and 4 *Gad2-cre* (orange) mice, graphed together with the original 4 *Sert-cre* (blue) and *Gad2-cre* (red) experiments. Data are shown as the proportion of total cells counted in the 6 regions. The cortex and medulla make up a larger proportion of inputs to serotonergic neurons while the CeA and BNST make up a larger proportion of inputs to GABA neurons. For statistical analysis, we combined the new brains with the original 8 and performed 2-tailed t-tests followed by Holm-Sidak corrections for multiple comparisons.

Supplemental Experimental Procedures

Rabies-mediated Transsynaptic Tracing

To restrict starter cells to serotonin or GABA neurons, we performed our tracing experiments in *Sert-cre* (Gong et al., 2007) and *Gad2-cre* (Taniguchi et al., 2011) mice, respectively. *Sert* encodes the plasma membrane serotonin transporter and *Gad2* encodes one of the two glutamic acid decarboxylases. For rabies tracing experiments, 4-6 week old mice were anesthetized with 65 mg/kg ketamine and 13 mg/kg xylazine (Lloid Laboratories) via intra-peritoneal injection, and 0.35 µl of a 1:1 mixture of AAV *CAG-FLEx-RG* and AAV *CAG-FLEx-TC* (*TC*^{B} or *TC*^{66T}) was injected using a stereotactic apparatus (KOPF). AAV serotype 5 was used for *TC*^{B}, AAV serotype 8 for *RG*, and AAV serotype 2 for *TC*^{66T}. For DR injections, we targeted directly on the midline at the midpoint between lambda and the posterior-most point of the sagittal suture. After carefully thinning the skull and removing the piece of bone over that location, we lowered the injection needle 3.3 mm (Z) from the surface of the blood vessel located below that area. After recovery, mice were housed on a regular 12-hour light/dark cycle with food and water ad-libitum. Two weeks later, 0.35 µl of EnvA-pseudotyped rabies virus was injected into the same brain location using the same procedure as above. After recovery, mice were housed in a biosafety level 2 (BSL2) facility for 5 days to allow for rabies spread and GFP expression.

Histology and Imaging

After 5 days of rabies infection, animals were perfused transcardially with phosphate buffered saline (PBS) followed by 4% paraformaldehyde (PFA). Brains were dissected, post-fixed in 4% PFA for 12-24 hours, and placed in 30% sucrose for 24-48 hours. They were then embedded in Optimum Cutting Temperature (OCT, Tissue Tek) and stored at in the -80ºC freezer until sectioning. For the antibody staining in Figure 1 and Figure S1, 40-µm floating sections were collected into PBS. They were then washed 3x10 min in PBS and blocked for 2-3 hours at room temperature (RT) in 10% normal donkey serum (NDS) in PBS with 0.3% Triton-X100 (PBST). Primary antibody (Millipore, rabbit anti-Tph2) was diluted 1:1000 in 5% NDS in PBST, and incubated for two nights at 4-degrees. After 3x10 min washes, secondary antibody was applied for 2-3 hours at room temperature (donkey anti-rabbit, Alexa-647, Jackson ImmunoResearch), followed by 3x10min washes in PBST. Sections were additionally stained with DAPI (1:10,000 of 5 mg/mL, Sigma-Aldrich) in PBS for 10-15 min, and washed once more with PBS prior to mounting onto Superfrost Plus slides and coverslipping with Fluorogel (Electron Microscopy Sciences). These sections were then imaged using a Zeiss 780 confocal microscope, and images were processed using NIH ImageJ software. For antibody staining shown in Figures 7, S1 (mouse anti-S100B, Sigma, cat#S2532) and S5, the same procedure was used as described above except we used 60-µm floating sections, 3-4 nights in primary, and 24 hours in secondary at 4-degrees.

For long-range tracing analysis (Figures 2-5, 8), consecutive 60-µm coronal sections were collected onto Superfrost Plus slides and stained for NeuroTrace Blue (NTB, Invitrogen). For NTB staining, slides were washed 1x5 min in PBS, 2x10 min in PBST, incubated for 2-3 hours at RT in (1:500) NTB in PBST, washed 1x20 min with PBST and 1x5min with PBS. Sections were additionally stained with DAPI (1:10,000 of 5 mg/mL, Sigma-Aldrich), which was included in the last PBST wash of NTB staining. Whole slides were then imaged with a 5x objective using a Leica Ariol slide scanner with the SL200 slide loader.

Rabies Tracing Combined with in situ Hybridization (ISH)

To make ISH probes, DNA fragments of 400-1000 bp containing the coding or untranslated region sequences were amplified by PCR from mouse whole brain cDNA (Zyagen) and subcloned into pCR-BluntII-topo vector (Life Technologies, cat# K2800-20). T3 RNA polymerase recognition site (AATTAACCCTCACTAAAGGG) was added to the 3'-end of the PCR product. Primer sets used in the present study are listed below. Plasmids were then amplified, the insert removed via EcoRI (New England Biolabs, cat#R0101L) digest, and purified using a PCR purification kit (QIAGEN, cat#28104). 500-1000 ng of the DNA fragment was then used for *in vitro* transcription by using DIG RNA labeling mix (cat#11277073910) and T3 RNA polymerase (cat#11031163001) according to the manufacture's instruction (Roche Applied Science). After DNase I (Roche Applied Science, cat#04716728001) treatment for 30 min at 37^{o}C, the RNA probe was purified by ProbeQuant G-50 Columns (GE Healthcare, cat# 28-9034-08) according to the manufacture's instructions.

For TC^{B}-based tracing combined with in situ hybridization, 60-µm consecutive sections were collected onto Superfrost slides (no-coating, Fisher Scientific, cat#22-034-980), dried, and stored at –80^{o}C until use. Specific slides were then thawed and viewed on a Zeiss compound fluorescence microscope, and the sections containing regions of interest were recorded. Those sections were then floated off using PBS into wells of a 24-well plate for use with multiple probes. The sections were fixed for 15 min in 4% paraformaldehyde in PBS at room temperature, rinsed with PBS, and incubated with 7µg/ml Proteinase K (Life Technologies, cat#25530-049) in 10 mM Tris-Cl, pH 7.4, 1 mM EDTA for 10 min at 37°C. After fixing again with 4% paraformaldehyde in PBS for 10 min and rinsing with PBS, the sections were incubated with 0.25% acetic anhydride in 0.1 M triethanolamine, pH 8.0, for 15 min and washed with PBS. Probes were diluted (~1:1000) with the hybridization buffer (50% formamide, 10mM Tris-Cl pH 8.0, 200µg/ml tRNA, 10% Dextran Sulfate, 1x Denhalt's solution, 600mM NaCl, 0.25% SDS), mixed well, preheated at 85^{o}C for 5 min, and applied to each well (300-500 µl/well). After 16-20h of incubation at 50°C, the sections were washed, first with 2× SSC-50% formamide, then with 2× SSC, and finally with 0.2× SSC twice for 20 min at 65°C. After blocking for 1-2h with the 1% blocking reagent (Roche Applied Science, cat#10057177103), sections were incubated with alkaline phosphatase-conjugated anti-DIG antibody (1:1000, Roche Applied Science, cat# 1093274) and chicken anti-GFP antibodies (1:500; Aves Labs, cat#GFP-1020) overnight at 4^{o}C. After washing with Roche Wash Buffer (cat#11585762001) three times for 15 min followed by rinsing with the detection buffer (100mM Tris-Cl pH8.0, 100mM NaCl, 10mM $MgCl_2$), probe-positive cells were detected by Fast Red TR/Naphthol AS-MX Tablets (Sigma-Aldrich, cat#F4523). After washed with Roche Wash Buffer three times for 10 min, sections were incubated with FITC conjugated donkey anti-chicken antibodies (1:200; Jackson ImmunoResearch) for an additional 1-2h, and washed with PBS three times for 10 min. Finally the sections were treated with PBS containing 4',6-diamidino-2-phenylindole dihydrochloride (DAPI; Sigma-Aldrich, Cat#D8417) for 20 min and mounted with cover glass using Fluorogel (Electron Microscopy Sciences, Cat#17985-10). Sections were imaged with a Nikon CCD camera by using a 5 or 10x objective, Leica Ariol slide scanner, or by confocal microscopy (Zeiss 780). Images were processed in ImageJ. We used FIJI and the cellcounter plugin to quantify overlap. For CeA and PVH quantifications, we alternated sections between probes, with an average of every 3rd section with the same probe in the CeA, and every 2nd section for the PVH.

For TC^{66T}-based tracing combined with in situ hybridization, we found that most of the mCherry signal from TC^{66T} was quenched during the process, but that a small amount remained, making it difficult to discern GABA+ presynaptic partners from serotonin starter cells. Therefore, the protocol was performed as described above with one exception. For the first ~2/3 of our experiments, prior to the beginning in situ hybridization, we imaged consecutive sections so that we could *post-hoc* identify the region covered by starter cells and exclude them from our analysis. We later found that staining with rat anti-mCherry (Life Technologies, cat# M11217, 1:500) during *in situ* as described above for GFP staining, followed by Alexa 647-conjugated Goat anti-rat secondary (1:500; Jackson ImmunoResearch, cat#112-605-167) allowed us to identify starter cells without the difficulties of pre-imaging and *post-hoc* analysis.

For the co-expression analysis of *vGlut2* and *oxytocin* or *vasopressin* (Figure 4E), *vGlut2-cre* mice (Vong et al., 2011) were crossed to nuclear-GFP cre-reporter mice (Stoller et al., 2008), and coronal sections through the PVH were used for ISH for *oxytocin* or *vasopressin* combined with GFP antibody staining, as described above. In situs were imaged using a Zeiss 780 confocal microscope, and images were processed using NIH ImageJ software.

Channelrhodopsin-Assisted Circuit Mapping

For electrophysiological recordings from brain slices, we used adult *Sert-cre* or *Gad2-cre* mice (8-12 weeks). 0.075 µl of AAV_{DJ}-*CaMKIIa-ChR2(H134R)-EYFP* was injected at 3 positions along the medial-lateral axis: 0.5, 1.5, and 2.5 mm from the midline, all 2.22mm anterior to the bregma, and at three depths for each of these positions: 3mm, 2mm, 1mm. 4 weeks following AAV injection, 0.5 µl of AAV_{DJ}-*Ef1a-FLEx-mCherry* was injected into the DR using the procedure described above. Two weeks later, acute coronal brain sections of the DR were sliced for electrophysiological experiments.

The methods of slice preparation and physiological recordings were similar to previous study (Ren et al., 2011). Briefly, adult mice were deeply anesthetized with intraperitonial (i.p.) injection of avertin (300 mg/kg) and transcardially perfused with ~5 ml of ice-cold oxygenated solution containing (in mM): 225 sucrose, 119 NaCl, 2.5 KCl, 1 NaH_2PO_4, 4.9 $MgCl_2$, 0.1 $CaCl_2$, 26.2 $NaHCO_3$, 1.25 glucose, 3 kynurenic acid, and 1 Na-ascorbate (all chemicals were from Sigma, St Louis, MO, USA). Mice were then rapidly decapitated and whole brains were dissected into ice-cold oxygenated slicing solution, including (in mM) 110 choline chloride, 2.5 KCl, 0.5 $CaCl_2$, 7 $MgCl_2$, 1.3 NaH_2PO_4, 1.3 Na-ascorbate, 0.6 Na-pyruvate, 20 glucose, and 25 $NaHCO_3$ (saturated with 95% O_2 and 5% CO_2). Coronal brain sections (250 µm thickness) containing DR were cut with a vibratome (VT1000s, Leica, Nussloch, Germany). Slices were incubated for at least 1 hr at 34°C in oxygenated artificial cerebrospinal fluid (aCSF) containing (in mM) 125 NaCl, 2.5 KCl, 2 $CaCl_2$, 1.3 $MgCl_2$, 1.3 NaH_2PO_4, 1.3 Na-ascorbate, 0.6 Na-pyruvate, 20 glucose, and 25 $NaHCO_3$. They were then transferred to a recording chamber on an upright Olympus fluorescent microscope equipped with differential interference contrast optics (DIC, COHU 4915–2000). During recording, slices were submerged and superfused (2 ml/min) with aCSF at room temperature (24-26°C).

Whole-cell recordings from DR serotonin and GABA neurons were obtained under visual control of DIC microscopy. Recording pipettes (3.5-4.5 MΩ) were backfilled with internal solution containing Cs^+, TEA and QX-314 to block K^+ and Na^+ channels. For the verification of the rectified GABA neuron I/V curve, 0.1 mM spermine was add into the internal solution. Detailed protocol lists as the following (in mM): 125 Cs-gluconate, 10 HEPES, 0.6 EGTA, 3 Na_2ATP, 0.3 Na_3GTP, 4 $MgCl_2$, and 10 Na_2phosphocreatine, 5 QX-314, 10 TEA, (0.1 spermine).

The pH was adjust to 7.2–7.4 by adding CsOH. Voltage-clamp and current-clamp recordings were carried out with a computer-controlled amplifier (MultiClamp 700B, Molecular Devices). For voltage-clamp recordings, neurons were held at -65 mV. Traces were low-pass filtered at 1.2 (voltage clamp) or 2.6 kHz (current clamp) and digitized at 10 kHz (DigiData 1440, Molecular Devices). Data were acquired by Clampex 10.4 and analyzed using Clampfit 10.4 software (Molecular Devices).

For photostimulation of axon terminals of anterior cortical neurons in DR, an optical fiber (150 μm core diameter, NA = 0.22) coupled to a diode-pumped solid-state 473 nm laser was submerged in aCSF and placed ~300 μm from the recording site. Delivery of optical pulses was controlled by a laser driver (Crystalaser, CL-2005) and digital commands from the Digidata 1440. For drug-application, DNQX (10 μM), picrotoxin (50 μM), or APV (50 μM) were added to the superfusion medium by dilution of a stock solution.

To quantify EPSC amplitudes, at least five minutes of baseline were collected from each cell. Cells were tested with optical stimulations at fixed intervals of 20 or 30 s before and during the application of DNQX, APV, TTX or 4-AP, and six sweeps of EPSCs were averaged for each data point. Drug effects were measured by recording traces 5 min before and 15 min after drug perfusion. The amplitudes of EPSCs were measured by taking the mean of a 2-3 ms window around the peak and subtracting this with the mean of a 10 ms window immediately before the stimulation. We only analyzed light stimulated EPSCs that were reliably produced by light stimulation, which exhibited an average amplitude >20 pA. The EPSC decay time was measured by the time interval between 90% and 10% peak amplitudes. The EPSC latency was calculated by the time interval between the command of DigiData 1440 and the peak of EPSC. Summary data are presented as mean ± SEM. Paired t-tests were carried out to detect statistical difference for each manipulation.

To label neuronal morphology, cells were filled with Neurobiotin (0.25%; Vector Laboratories) included in the intrapipette recording solution. After recordings, brain slices were fixed with 4% paraformaldehyde in 0.1M PBS and stained with streptavidin (DyLight 405, Jackson ImmunoResearch; 1:500, 12hr at 4°C) in 0.1M PBS with 0.3% Triton-X. *Gad2-cre* brain slices were stained with anti-Tph2 antibody after recording and imaged as previous described.

PCR Primers used to Prepare Templates for ISH Probes

The following primers were used to amplify the templates for ISH probes. In some cases, we designed multiple ~900bp probes for a single mRNA and mixed probes to amplify the ISH signals. T3 polymerase recognition site is indicated by underline.

Preproenkephalin

5’-GACAGCAGCAAACAGGATGA; 5’-
AATTAACCCTCACTAAAGGGTTTCGTCAGGAGAGATGAGG

vGlut1

5’-CTGGCAGTGACGAAAGTGAA; 5’-
AATTAACCCTCACTAAAGGGACACAACAAATGGCCACTGA

vGlut2

5’-CTCCCCCATTCACTACCTGA; 5’-
AATTAACCCTCACTAAAGGGGGTCAGGAGTGGTTTGCATT

vGlut3

5’-AGCAACTCCTCACTCAGCTT; 5’-
AATTAACCCTCACTAAAGGGCCCAGCATAGGAACCACAGA

5’-TAGGAGAAGGGGCCAACTTG; 5’-
AATTAACCCTCACTAAAGGGTGGGTGCGATACTTCCAGTT
Gad1
5’-CACAAACTCAGCGGCATAGA; 5’-
AATTAACCCTCACTAAAGGGGGACGAGCAACATGCTATGG
Gad2
5’-GGGATGTCAACTACGCGTTT; 5’-
AATTAACCCTCACTAAAGGGTGCATCAGTCCCTCCTCTCT
5’-CTCCAATCCCCTTCTTCTCC; 5’-
AATTAACCCTCACTAAAGGGTGTGCATCCTTTGTCCATGT
Oxytocin
5’-TGGCTTACTGGCTCTGACCT; 5’-
AATTAACCCTCACTAAAGGGAGGAAGCGCGCTAAAGGTAT
Vasopressin
5’-CGCTCACAGAGCTCTTCCTT; 5’-
AATTAACCCTCACTAAAGGGGACACCAGGGTGCAGTTTTT
Crh
5’-TTCTCCCCCACCTTCTCTCT; 5’-
AATTAACCCTCACTAAAGGGACTGGATGACTCCCATCTGC
Pkc∂
5’-CCTCAAGCTGGACAATGTGA; 5’-
AATTAACCCTCACTAAAGGGAGGGAAGGCAAATTCACAAA
Tac1
5’-CGCAAAATCGAACATGAAAA; 5’-
AATTAACCCTCACTAAAGGGTCACGAAACAGGAAACATGC
Tac2
5’-AGGGAGGGAGGCTCAGTAAG 5’-
AATTAACCCTCACTAAAGGGTTGCTATGGGGTTGAGGCTG

3D Reconstruction

For 3D reconstruction (Figure S2), whole-slide images of scanned slides were imported into custom Matlab software to segment images into individual brain sections based on the NTB stain. To accelerate processing, the full resolution images (xy-resolution=1.29 μm/pixel) were initially downsampled by a factor of 32 in both x- and y- dimensions. Segmentation included the application of a mask fit to the edge of each section to remove all image features outside the section. Background subtraction and contrast enhancement of the NTB channel were then applied. The processed NTB images for each section were then serially registered using a combination of automated and manual methods. All transformations were rigid (rotation and translation only). Automated alignment used Matlab's Image Processing Toolbox functions for intensity-based image registration with Mattes mutual information as the optimization metric. Manual registration was performed using a custom user interface. To construct brain volumes, the section masks and registration transformations were scaled and applied to higher resolution images of all channels. The final volumes were down-sampled from full resolution by a factor of 4 in both x- and y-dimensions to facilitate agile manipulation of the complete volume. The final volume resolution was 5.15 x 5.15 x 60 μm/voxel (xyz). The volumes were exported in a standard image format and were further processed and analyzed in ImageJ and Imaris (Bitplane,

Zurich).

Supplemental References

Gong, S., Doughty, M., Harbaugh, C.R., Cummins, A., Hatten, M.E., Heintz, N., and Gerfen, C.R. (2007). Targeting Cre recombinase to specific neuron populations with bacterial artificial chromosome constructs. J Neurosci *27*, 9817-9823.

Holloway, B.B., Stornetta, R.L., Bochorishvili, G., Erisir, A., Viar, K.E., and Guyenet, P.G. (2013). Monosynaptic glutamatergic activation of locus coeruleus and other lower brainstem noradrenergic neurons by the C1 cells in mice. J Neurosci *33*, 18792-18805.

Miyamichi, K., Shlomai-Fuchs, Y., Shu, M., Weissbourd, B.C., Luo, L., and Mizrahi, A. (2013). Dissecting local circuits: parvalbumin interneurons underlie broad feedback control of olfactory bulb output. Neuron *80*, 1232-1245.

Petreanu, L., Huber, D., Sobczyk, A., and Svoboda, K. (2007). Channelrhodopsin-2-assisted circuit mapping of long-range callosal projections. Nat Neurosci *10*, 663-668.

Petreanu L, Mao T, Sternson SM, Svoboda K. (2009) The subcellular organization of neocortical excitatory connections. Nature *457,* 1142–1145.

Ren, J., Qin, C., Hu, F., Tan, J., Qiu, L., Zhao, S., Feng, G., and Luo, M. (2011). Habenula "cholinergic" neurons co-release glutamate and acetylcholine and activate postsynaptic neurons via distinct transmission modes. Neuron *69*, 445-452.

Stoller, J.Z., Degenhardt, K.R., Huang, L., Zhou, D.D., Lu, M.M., and Epstein, J.A. (2008). Cre reporter mouse expressing a nuclear localized fusion of GFP and beta-galactosidase reveals new derivatives of Pax3-expressing precursors. Genesis *46*, 200-204.

Taniguchi, H., He, M., Wu, P., Kim, S., Paik, R., Sugino, K., Kvitsiani, D., Fu, Y., Lu, J., Lin, Y., *et al.* (2011). A resource of Cre driver lines for genetic targeting of GABAergic neurons in cerebral cortex. Neuron *71*, 995-1013.

Vong, L., Ye, C., Yang, Z., Choi, B., Chua, S., Jr., and Lowell, B.B. (2011). Leptin action on GABAergic neurons prevents obesity and reduces inhibitory tone to POMC neurons. Neuron *71*, 142-154.